 doi:10.20944/preprints202204.0115.v1

Article

A Quantum-Chemical Study of Boro-Fullerenes $B_{60}H_{60}$, $B_{60}F_{30}H_{30}$, and $B_{60}F_{60}$

Ofelia B. Oña [1], Maxime Ferrer [2,3], Diego R. Alcoba [4,5] , Alicia Torre [6], Luis Lain [6], Gustavo E. Massaccesi [7], Douglas J. Klein [8], Ibon Alkorta [2], José Elguero [2] and Josep M. Oliva-Enrich [9,*]

[1] Instituto de Investigaciones Fisicoquímicas Teóricas y Aplicadas, Universidad Nacional de La Plata, CCT La Plata, Consejo Nacional de Investigaciones Científicas y Técnicas, Diag. 113 y 64 (S/N), Sucursal 4, CC 16, 1900 La Plata, Argentina; ofelia@inifta.unlp.edu.ar
[2] Instituto de Química Médica (CSIC), 28006 Madrid, Spain; maxime.ferrer@iqm.csic.es ; ibon@iqm.csic.es ; iqmbe17@iqm.csic.es
[3] PhD Programme in Theoretical Chemistry and Computational Modelling, Doctoral School, Universidad Autónoma de Madrid, 28049 Madrid, Spain
[4] Departamento de Física, Facultad de Ciencias Exactas y Naturales, Universidad de Buenos Aires, Ciudad Universitaria, 1428 Buenos Aires, Argentina; dalcoba@df.uba.ar
[5] Instituto de Física de Buenos Aires, Consejo Nacional de Investigaciones Científicas y Técnicas, Ciudad Universitaria, 1428 Buenos Aires, Argentina
[6] Departamento de Química Física, Facultad de Ciencia y Tecnología, Universidad del País Vasco, Apdo. 644, E-48080 Bilbao, Spain; alicia.torre@ehu.es ; luis.lain@ehu.es
[7] Departamento de Ciencias Exactas, Ciclo Básico Común, Universidad de Buenos Aires, Ciudad Universitaria, 1428 Buenos Aires, Argentina; gustavo@oma.org.ar
[8] Texas A&M University at Galveston, Galveston, TX 77550, USA; kleind@tamug.edu
[9] Instituto de Química-Física "Rocasolano" (CSIC), 28006 Madrid, Spain; j.m.oliva@iqfr.csic.es
* Correspondence: j.m.oliva@iqfr.csic.es; Phone No. +34-917459555

Abstract: The one-to-one structural correspondence between any conjugated hydrocarbon C_nH_m and the borane B_nH_{m+n} is extended here, with the B3LYP/cc-pVDZ model, to pure conjugated carbon systems with the example of buckminsterfullerene C_{60} with the corresponding icosahedral isoelectronic system *closo*-borane $B_{60}H_{60}$, and the fluorine substituted systems $B_{60}F_{30}H_{30}$ and $B_{60}F_{60}$, all with icosahedral I_h symmetry. All systems correspond to energy minima in the potential energy hypersurface, except for $B_{60}(F_{30})_{in}(H_{30})_{out}$. Selected electronic structure methods are used to characterize all systems: molecular electrostatic potentials (MEP), atomic charges, bond orders, and topological properties of the electron density within quantum theory of atoms-in-molecules (QTAIM) and electron-localization function (ELF) theory. In the particular case of $B_{60}H_{60}$ we use the recently developed Hückeloid model to characterize this system. The stability of the energy minimum icosahedral structure $B_{60}F_{60}$ could have an origin in F···F attractive interactions of the inner fluorine atoms of the cage.

Keywords: boron; fullerenes; chemical bond; electronic structure; DFT; localization; bond order; QTAIM ; ELF; Hückeloid model; heat of formation

1. Introduction

The recent discovery and isolation of planar (2D) hexagonal boron sheets – borophene polymorphs – and 2D hexagonal borane $(BH)_1$ – borophane polymorphs – suggests the possibility of creating a new 2D borane chemistry [1-4]. In much the same way as benzene is the repetition pattern in graphene, planar cyclohexaborane(12) with formula B_6H_{12} [5,6] – yet an unknown molecule – should be the repetition pattern for 2D borophane, wherein orbital vacancies are saturated with e.g. hydrogen atoms. Nowadays, boron chemistry [7] is classified according to (i) organoboron, and (ii) polyhedral heteroboranes. In (i), a few boron atoms appear in organic molecules and metal complexes, leading to a wide variety of reaction mechanisms and catalysis processes. In (ii), the molecules involved are open and closed polyhedral boranes, with some substitutions of boron atoms

Preprints (www.preprints.org) | NOT PEER-REVIEWED | Posted: 13 April 2022 doi:10.20944/preprints202204.0115.v1

by heteroatoms and metals. For the case (ii) the usual known reaction mechanisms of organic chemistry cannot be applied given the complex many-electron multicenter bonding in the clusterized boranes, since there are no transferability patterns as in organic chemistry. For instance, the *ortho*/*para* directors in the electrophilic aromatic substitution in aniline Ph-NH_2 do not apply for the icosahedral aminocarborane 1-NH_2-1,2-$C_2B_{10}H_{11}$ [8], if we put forward the "structural analogy" between planar benzene and the icosahedral *ortho*-, *meta*- and *para*-carboranes [9].

On the other hand, a simple link between hydrocarbon and borohydride (borane) chemistries [5] can be drawn, in particular within conjugated hydrocarbon chemistry [10,11]: $C_nH_m \leftrightarrow B_nH_{m+n}$; namely, to any planar or non-planar conjugated hydrocarbon C_nH_m there corresponds an isostructural and isoelectronic borane B_nH_{m+n}. This transformation is easily carried out by substituting all C=C double bonds by the $B(H_2)B$ central moiety in diborane(6). Up to date, all transformations of known conjugated hydrocarbons lead to the same structures as compared to the equivalent boranes [10,11]. However, with the exception of the ethylene ↔ diborane(6) and the 2D graphene ↔ 2D $(BH)_1$ borophane sheet correspondences, most of these planar boranes do not exist or have not yet been isolated. As mentioned at the beginning of this section, the isolation of planar 2D hexagonal borophene and borophane $(BH)_1$ sheets might be the starting point for creating a new 2D boron chemistry.

The possibility of carrying out the $C_nH_m \leftrightarrow B_nH_{m+n}$ transformation for m = 0, namely conjugated carbon structures without H atoms, is the case in point in this work. A straight example is the well known buckminsterfullerene C_{60} [12], an icosahedral 3D cage with conjugation all around the sphere, with the corresponding $C_n \leftrightarrow B_nH_n$ transformation with n = 60, i.e. $C_{60} \leftrightarrow B_{60}H_{60}$. The three-dimensional concatenation of diborane(6) into a fullerene structure $B_{60}H_{60}$ with the same symmetry, I_h, and number of electrons, n = 360, as compared to C_{60}, leads to two different types of bridge hydrogens in the $B(H_2)B$ moiety: H_{out} and H_{in} , with hydrogen atoms radially outside or inside the B_{60} spherical cage respectively. Substitution of hydrogen atoms by fluorine atoms and conserving the icosahedral I_h symmetry, leads to systems $B_{60}F_{60}$, $B_{60}(F_{30})_{in}(H_{30})_{out}$, and $B_{60}(F_{30})_{out}(H_{30})_{in}$, as shown in Figure 1. There has been some previous efforts to devise *closo*-borane analogs of C_{60} with the $B_{60}H_{60}$ structure [13,14] – characterized with local density functional methods – and some with pure boron cages [15-18] by introducing B atoms to make triples of B atoms with 3-center bonding, while here we utilize $B(H_2)B$ multi-center bonding.

The goal of this work is to carry out a quantum-chemical study of the geometrical and electronic structure of these icosahedral *closo*-boranes and *closo*-fluoroboranes. In Section 2 and Section 3 we include the results and discussion respectively. The Computational Methods are included in Section 4, and finally in Section 5 we summarize the main conclusions of this work.

Preprints (www.preprints.org) | NOT PEER-REVIEWED | Posted: 13 April 2022 doi:10.20944/preprints202204.0115.v1

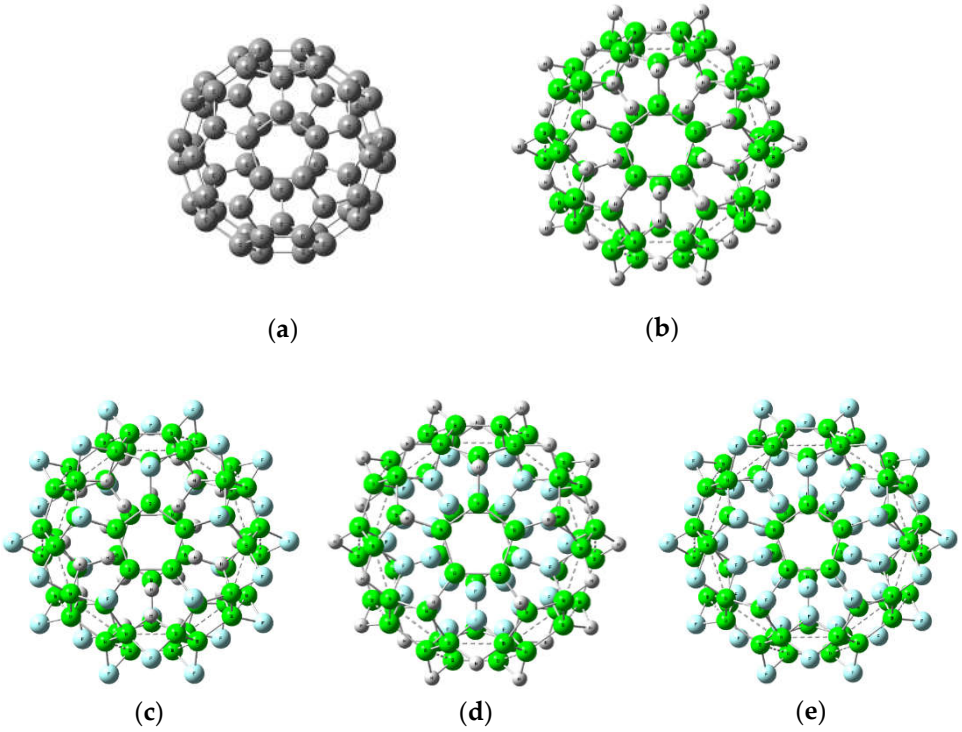

Figure 1. Optimized geometries in (a) C_{60} , (b) $B_{60}H_{60}$, (c) $B_{60}(F_{30})_{out}(H_{30})_{in}$, (d) $B_{60}(F_{30})_{in}(H_{30})_{out}$, and (e) $B_{60}F_{60}$ with the B3LYP/cc-pVDZ model. All structures have icosahedral I_h symmetry and correspond to energy minima except (d) $B_{60}(F_{30})_{in}(H_{30})_{out}$, which corresponds to a 7^{th}–order saddle point. The B···B long contacts are drawn with dashed lines.

2. Results

2.1. Geometries

In Figure 1 and Table 1 the structure and main geometrical parameters of the systems included in this work are collected. As for $B_{60}F_{30}H_{30}$, from now on this formula refers to $B_{60}(F_{30})_{out}(H_{30})_{in}$ from Figure 1d since the alternative structure $B_{60}(F_{30})_{in}(H_{30})_{out}$ is a 7^{th}-order saddle point, see Figure 1(e). All these molecules have icosahedral I_h symmetry, as in the fullerene C_{60}. In Table 1 bond lengths and angles are gathered for these molecules. On one hand, $B_{60}H_{60}$, $B_{60}F_{30}H_{30}$, and $B_{60}F_{60}$ show two different types of B–B bond lengths, one from 1.871 Å (in $B_{60}H_{60}$) to 2.389 Å (in $B_{60}F_{60}$) corresponding to joining two six-membered rings (6MR), and another B-B bond length from 1.736 Å (in $B_{60}F_{30}H_{30}$) to 1.781 Å (in $B_{60}F_{60}$), corresponding to joining a 6MR with a five-membered ring (5MR). In fullerene C_{60}, the C-C bond length corresponding to the fusion of two 6MRs is 1.398 Å, and the other corresponding to the fusion of a 6MR and a 5MR is 1.456 Å. On the other hand, the B-H_{in} (B-F_{in}) and B-H_{out} (B-F_{out}) bond lengths, with the hydrogen (fluorine) inside and outside the boron cage, respectively, in 4-atom rhombus are quite similar. In $B_{60}H_{60}$, the B-H-B angles are 90º but the B-F-B angles are slightly larger up to 95º in $B_{60}F_{60}$. In $B_{60}F_{30}H_{30}$, the asymmetry in the 4-atom rhombus given by H and F (inside/outside the boron cage, respectively) is shown in the bond lengths and angles, with a B-F bond length of 1.570 Å, a B-H bond length of 1.344 Å, and a B-F-B angle of 81º, and a B-H-B angle of 99º. The Cartesian coordinates of the optimized geometries for these molecules are gathered in the SI file.

Preprints (www.preprints.org) | NOT PEER-REVIEWED | Posted: 13 April 2022 doi:10.20944/preprints202204.0115.v1

Table 1. Selected symmetry-unique geometrical parameters for C_{60}, $B_{60}H_{60}$, $B_{60}F_{30}H_{30}$ and $B_{60}F_{60}$ molecules optimized with the B3LYP/cc-pVDZ method. The distances and angles are given in ångström (Å) and degree respectively. All structures correspond to energy minima and have icosahedral I_h symmetry.

C_{60}	$B_{60}H_{60}$	$B_{60}F_{30}H_{30}$	$B_{60}F_{60}$
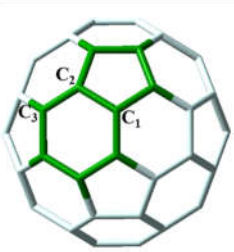	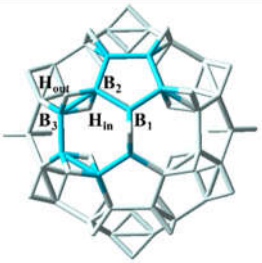	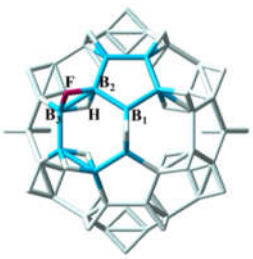	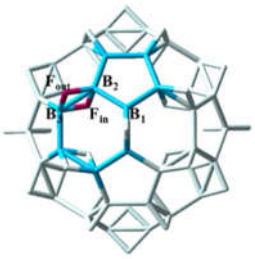
C_1C_2 1.456	B_1B_2 1.748	1.736	1.781
C_2C_3 1.398	B_2B_3 1.871	2.037	2.389
	B_2H_{out} 1.353	B_2F 1.570	B_2F_{out} 1.627
	B_2H_{in} 1.314	B_2H 1.344	B_2F_{in} 1.575
	$\angle B_2H_{out}B_3$ 87.5	$\angle B_2FB_3$ 80.9	$\angle B_2F_{out}B_3$ 94.5
	$\angle B_2H_{in}B_3$ 90.8	$\angle B_2HB_3$ 98.5	$\angle B_2F_{in}B_3$ 98.7
	$\angle H_{in}B_2H_{out}$ 90.9	$\angle FB_2H$ 90.3	$\angle F_{in}B_2F_{out}$ 83.4

2.2. Molecular electrostatic potentials

The Molecular Electrostatic Potential (MEP), $V(r)$, is defined as the interaction energy between the charge distribution of a molecule and a positive unit charge. Within quantum chemistry, the MEP is defined as the expectation value of the $\hat{r}^{-1}$ operator,

$$V(r) = \langle \Psi | \hat{r}^{-1} | \Psi \rangle$$

where Ψ stands for the molecular (nuclear + electronic) wavefunction [19]. Plots of MEP for C_{60} , $B_{60}H_{60}$, $B_{60}F_{60}$ and $B_{60}F_{30}H_{30}$ projected on the 0.001 au electron density isosurface in 3D and half-slice cut, are displayed in the 1st and 2nd rows of Figure 2 respectively. Red areas (V < 0) of the MEP are positive charge attractors (protons, cations and electrophiles), and blue areas (V > 0) of the MEP correspond to negative charge attractors (anions and nucleophiles).

The MEPs projected on the electron density isosurface show interesting features: in C_{60}, blue areas – negative charge attractors – appear above pentagonal (5MB) and hexagonal (6MB) faces; however, in $B_{60}H_{60}$, blue areas appear only above the BHB moieties, with slight red areas above pentagons and hexagons. The corresponding half-slice cut 2D projections show blue areas around and inside the C_{60} and $B_{60}H_{60}$ molecules, an indication that (poly)anion formation should be favorable, and the reason of why $C_{60}^{(n-)}$ anions are so stable [20,21]. For $B_{60}F_{30}H_{30}$ there are strong blue areas above the pentagons with slight red color areas above the BFB moieties. As for $B_{60}F_{60}$, the blue areas are even stronger above pentagons and strong red areas appear on the BFB moieties. An interesting feature of the half-slice cut in $B_{60}F_{60}$ is the inner and outer red areas which are positive charge attractors; the outer area is located on the fluorine atoms due to their lone pairs and the more electronegative nature of fluorine versus boron.

Preprints (www.preprints.org) | NOT PEER-REVIEWED | Posted: 13 April 2022 doi:10.20944/preprints202204.0115.v1

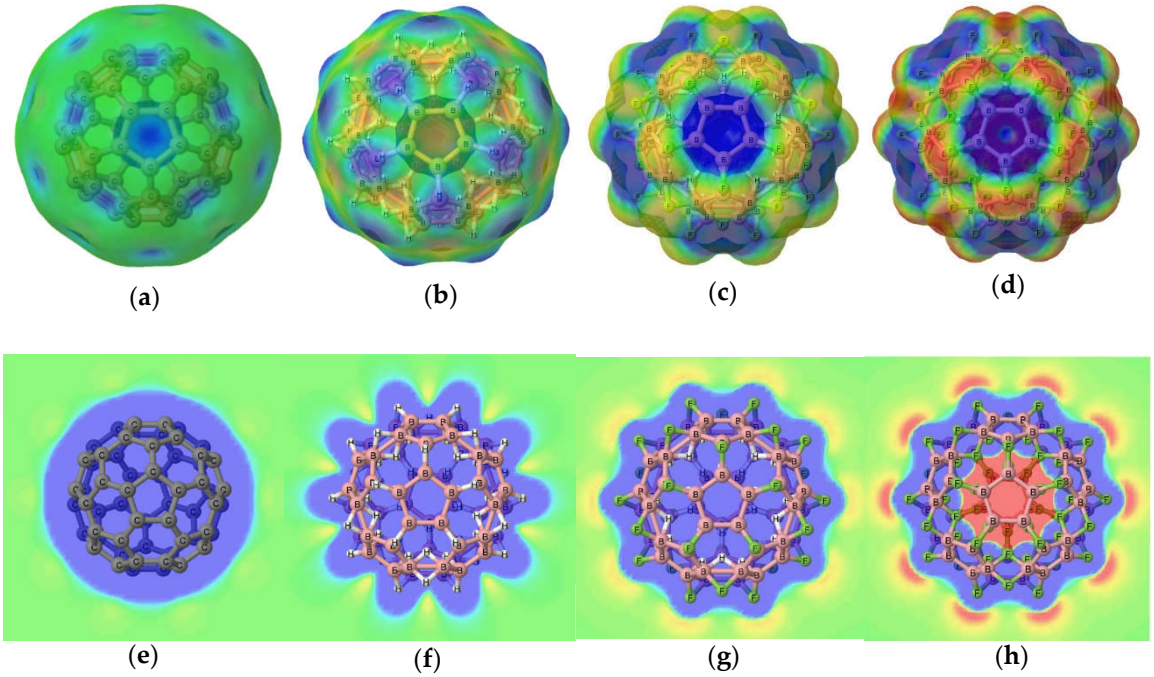

Figure 2. Plots of molecular electrostatic potentials (MEP) on top of electron density for (a) C_{60}, (b) $B_{60}H_{60}$, (c) $B_{60}F_{30}H_{30}$ and (d) $B_{60}F_{60}$. MEP on electron density half-slice cut 2D projection: (e) C_{60}, (f) $B_{60}H_{60}$, (g) $B_{60}F_{30}H_{30}$ and (h) $B_{60}F_{60}$. Values used for MEP plots: -0.015 au (red) ≤ V(r) ≤ +0.015 au (blue). Electron density cutoff ρ(r) = 0.001 au. B3LYP/cc-pVDZ computations.

2.3. Electronic structure: Atomic charges, bond orders and frontier orbitals

The atomic charges and bond orders of the four molecules, for several basis sets, are collected in Table 2, and calculated using the following equations [22]:

$$q_A = Z_A - \sum_{\mu \in A} (PS)_{\mu\mu} \qquad (2)$$

where q_A is the Mulliken atomic charge, Z_A is the atomic number of the atom A, P the one-particle density matrix, and S the overlap matrix. Two-center and three-center bond order indices [23-26] are obtained with Equation (3) and Equation (4) below respectively,

$$I_{AB} = \sum_{a \in A} \sum_{b \in B} (PS)_{ab} (PS)_{ba} \qquad (3)$$

and

$$I_{ABC} = \sum_{a \in A} \sum_{b \in B} \sum_{c \in C} (PS)_{ab} (PS)_{bc} (PS)_{ca} \qquad (4)$$

The atomic charges and bond order indices are gathered in Table 2 and the Foster-Boys localized molecular orbitals [27] are depicted in Figures 3-6. As shown in Table 2 in $B_{60}H_{60}$ the boron atoms provide charge to the hydrogen atoms – hydrogen is more electro-negative than boron – and the H_{in} and H_{out} atoms have very similar charges. However, in $B_{60}F_{30}H_{30}$ the boron atoms transfer charge to the hydrogen and fluorine atoms and the charge on F atoms is larger than that on the H atoms. In $B_{60}F_{60}$, the boron atoms provide charge to the fluorine atoms and the F_{in} and F_{out} have very similar charges. In C_{60}, the bond order indices are close to 1.0 for σ bonds and 1.5 for τ bonds (or banana bonds), constituting two-center two-electron (2c-2e) bonds, as shown in Figure 3. However, in $B_{60}H_{60}$ the three-center two-electron (3c-2e) bonds have indices close to 0.2 corresponding to τ bonds, as in the diborane molecule, a classical example for a (3c-2e) bond system, as

Preprints (www.preprints.org) | NOT PEER-REVIEWED | Posted: 13 April 2022 doi:10.20944/preprints202204.0115.v1

shown in Figure 4. Furthermore, (2c-2e) bond order index values close to 1.0, corresponding to σ bonds, are also shown by the $B_{60}H_{60}$ molecule as reflected in Figure 4. There are small values of (2c-2e) bond order indices, corresponding to σ bonds localized between a 6MR and a neighbor 6MR. The $B_{60}F_{30}H_{30}$ polyhedron also presents (3c-2e) bond index values close to 0.2, corresponding to τ bonds. (2c-2e) bond order index values about 1.0 and 0.5 for σ bonds are also shown by this molecule, as displayed in Figure 5. Similarly, the $B_{60}F_{60}$ molecule shows bond order index values close to 1.0 and 0.5 for σ bonds between a 6MR and a 4-atom rhombus sharing an edge and bonds on 4-atom rhombus, respectively. In this case no significant (3c-2e) bond indices are detected. The localized molecular orbitals of $B_{60}F_{60}$ are depicted in Figure 6, with no (3c-2e) bonds found; the three-center B-F_{out}-B and B-F_{in}-B moieties are described by two 2c-2e B-F bonds and the corresponding lone pairs, two for each F atom.

Table 2. Atomic charges q and multicenter bond order indices calculated at the Restricted Hartree-Fock (RHF) level of theory for several basis sets, with the optimized geometries of C_{60}, $B_{60}H_{60}$, $B_{60}F_{30}H_{30}$ and $B_{60}F_{60}$ molecules at the B3LYP/cc-pVDZ level of theory.

C_{60}

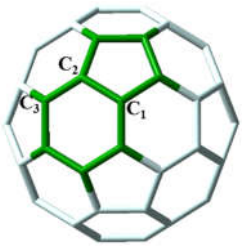

Multicenter	STO-3G	6-31G	cc-pVDZ
2c-2e (C_1C_2)	1.14	1.15	1.16
2c-2e′ (C_2C_3)	1.46	1.47	1.41

$B_{60}H_{60}$

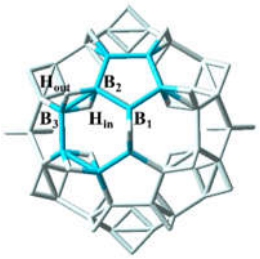

Charges	STO-3G	6-31G	cc-pVDZ
q(B)	0.055	0.053	0.002
q(H_{in})	-0.044	-0.059	0.071
q(H_{out})	-0.066	-0.047	-0.076
Multicenter	STO-3G	6-31G	cc-pVDZ
2c-2e (B_1B_2)	0.97	0.97	1.00
2c-2e′ (B_2B_3)	0.44	0.41	0.37
2c-2e′ (B_2H_{out})	0.48	0.46	0.49
2c-2e′ (B_2H_{in})	0.47	0.46	0.47
3c-2e ($B_2H_{in}B_3$)	0.21	0.22	0.24
3c-2e′ ($B_2H_{out}B_3$)	0.21	0.19	0.20

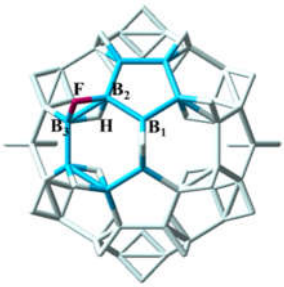

$B_{60}F_{30}H_{30}$

Charges	STO-3G	6-31G	cc-pVDZ
q(B)	0.114	0.299	0.166
q(H)	-0.090	-0.092	-0.061
q(F)	-0.138	-0.507	-0.272
Multicenter	STO-3G	6-31G	cc-pVTZ

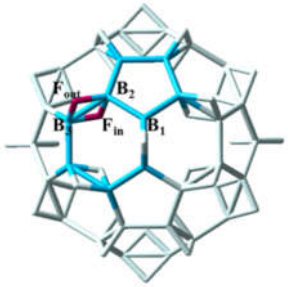

$B_{60}F_{60}$

Charges	STO-3G	6-31G	cc-pVDZ
q(B)	0.176	0.55	0.30
q(F_{in})	-0.175	-0.54	-0.26
q(F_{out})	-0.176	-0.55	-0.34
Multicenter	STO-3G	6-31G	cc-pVDZ

Preprints (www.preprints.org) | NOT PEER-REVIEWED | Posted: 13 April 2022 doi:10.20944/preprints202204.0115.v1

2c-2e (B_1B_2)	0.96	0.93	1.00	2c-2e (B_1B_2)	0.95	0.96	0.99
2c-2e′ (B_2B_3)	0.22	0.21	0.18	2c-2e′ (B_2B_3)	0.02	0.01	0.02
2c-2e′ (B_2H)	0.48	0.49	0.46	2c-2e′ (B_2F_{in})	0.61	0.34	0.55
2c-2e′ (B_2F)	0.64	0.36	0.51	2c-2e′ (B_2F_{out})	0.61	0.35	0.49
3c-2e (B_2HB_3)	0.20	0.22	0.19	3c-2e ($B_2F_{in}B_3$)	0.02	0.01	0.01
3c-2e′ (B_2FB_3)	0.02	0.02	0.03	3c-2e′ ($B_2F_{out}B_3$)	0.02	0.01	0.02

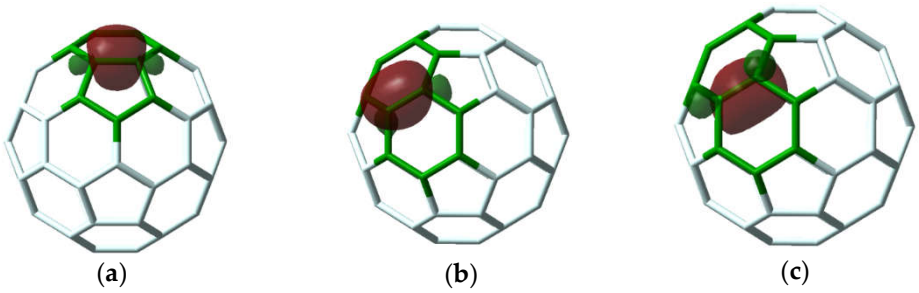

Figure 3. |0.06| (e/Bohr^3)$^{1/2}$ isosurfaces of Foster-Boys localized molecular orbitals for the C_{60} molecule at RHF/6-31G level of theory. (a) σ(2e-2c) = σ(C_1C_2), (b) τ_1(2c-2e) = τ_1(C_2C_3), (c) τ_2(2c-2e) = τ_2(C_2C_3). Only the valence orbitals were localized. Positive values are indicated in red and negative values in green.

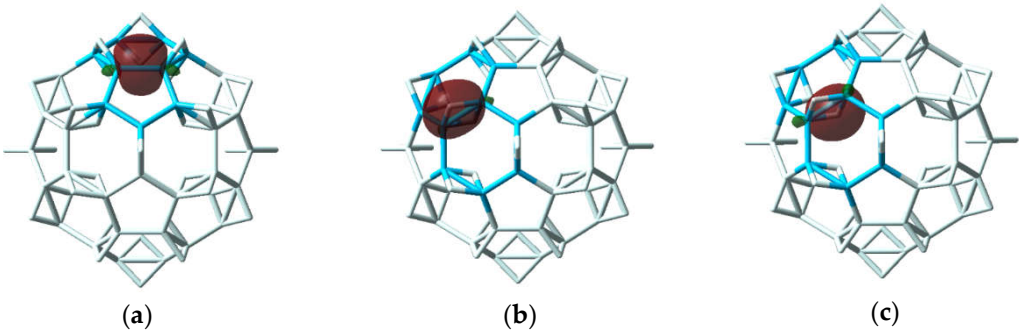

Figure 4. |0.06| (e/Bohr^3)$^{1/2}$ isosurfaces of Foster-Boys localized molecular orbitals for the $B_{60}H_{60}$ molecule at RHF/6-31G level of theory. (a) σ(2c-2e) = σ(B_1B_2), (b) τ_1(3c-2e) = τ_1($B_2H_{out}B_3$), (c) τ_2(3c-2e) = τ_2($B_2H_{in}B_3$). Only the valence orbitals were localized. Positive values are indicated in red and negative values in green.

Preprints (www.preprints.org) | NOT PEER-REVIEWED | Posted: 13 April 2022 doi:10.20944/preprints202204.0115.v1

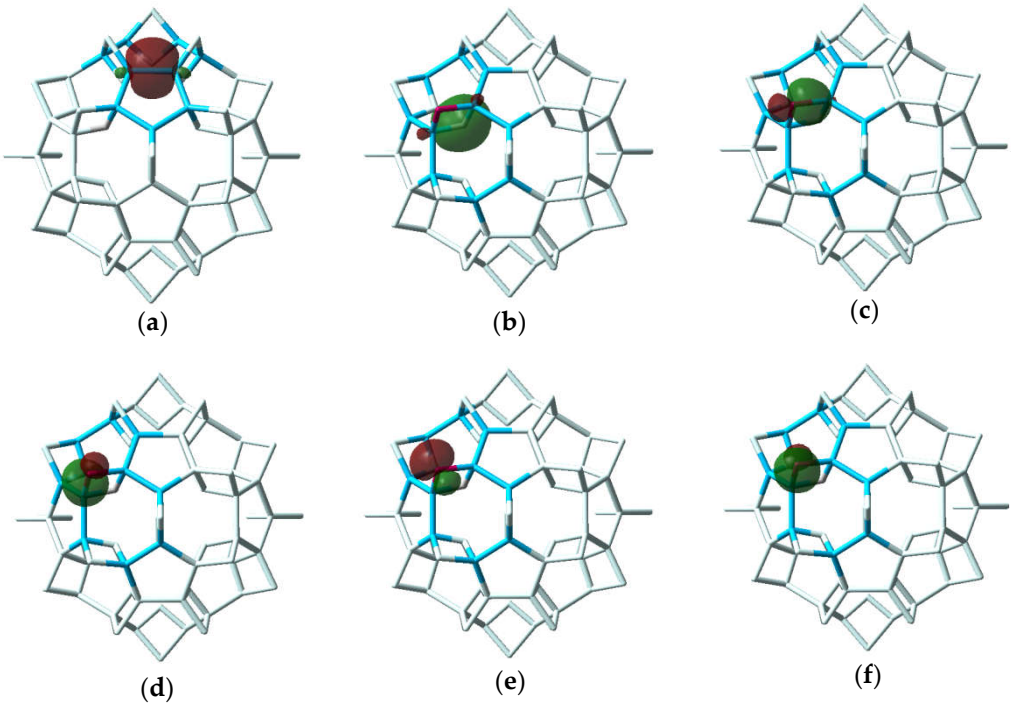

Figure 5. |0.06| $(e/Bohr^3)^{1/2}$ isosurfaces of Foster-Boys localized molecular orbitals for the $B_{60}F_{30}H_{30}$ molecule at RHF/6-31G level of theory. (a) σ(2c-2e) = σ(B_1B_2), (b) τ(3c-2e) = τ(B_2HB_3), (c) σ(2c-2e) = σ(FB_2), (d) σ(2c-2e) = σ(FB_3), (e) F lone pair 1, (f) F lone pair 2. Positive values are indicated in red and negative values in green.

Preprints (www.preprints.org) | NOT PEER-REVIEWED | Posted: 13 April 2022 doi:10.20944/preprints202204.0115.v1

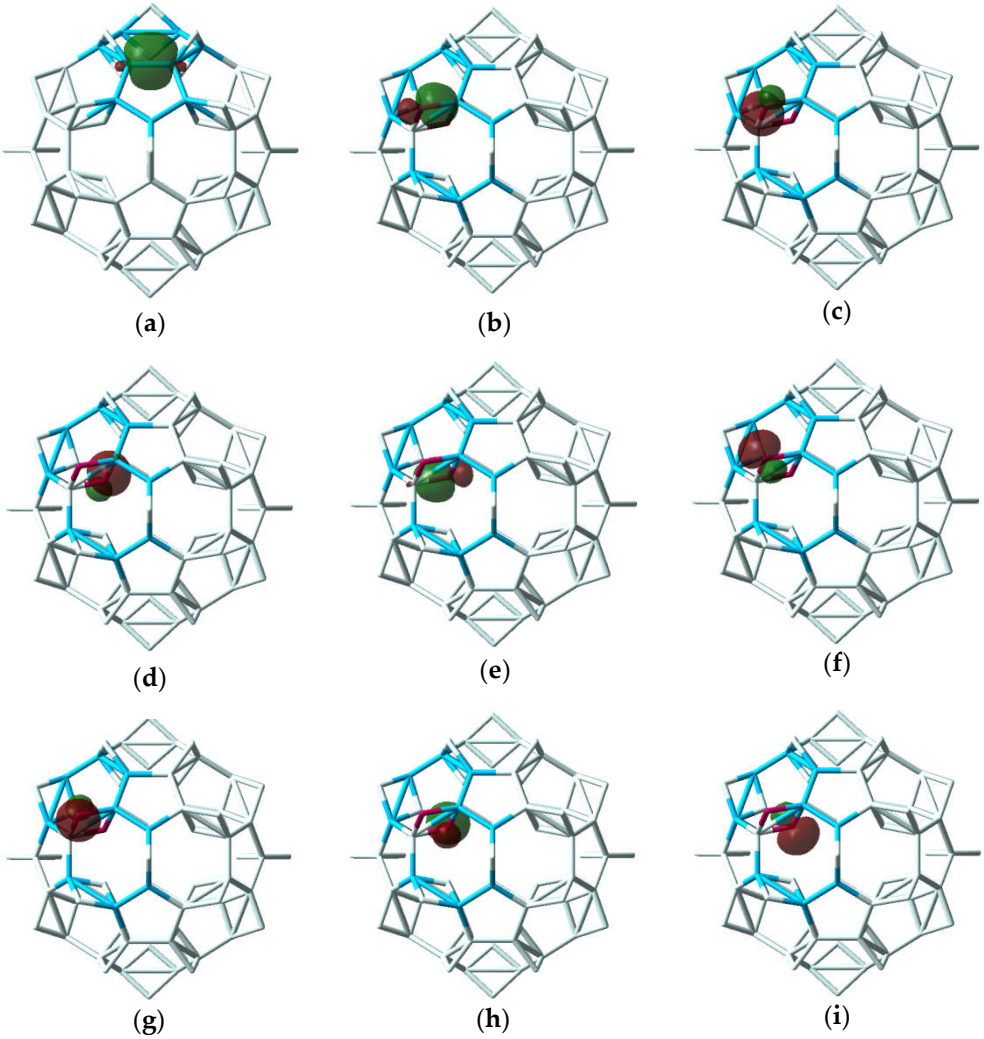

Figure 6. |0.06| (e/Bohr$_3$)$_{1/2}$ isosurfaces of Foster-Boys localized molecular orbitals for the $B_{60}F_{60}$ molecule at RHF/6-31G level of theory. (a) σ(2c-2e) = σ(B_1B_2), (b) σ(2c-2e) = σ($F_{out}B_2$), (c) σ(2c-2e) = σ($F_{out}B_3$), (d) σ(2c-2e) = σ($F_{in}B_2$), (e) σ(2c-2e) = σ($F_{in}B_3$), (f) F_{out} lone pair 1, (g) F_{out} lone pair 2, (h) F_{in} lone pair 1, (i) F_{in} lone pair 2. Positive values are indicated in red and negative values in green.

We now turn to orbital energy levels and frontier orbital analysis. The orbital energy levels around the frontier orbitals HOMO and LUMO in C_{60}, $B_{60}H_{60}$, $B_{60}F_{30}H_{30}$, and $B_{60}F_{60}$ systems with several basis sets for comparative purposes are depicted in Figure 7, with quantum-chemical computations at the RHF level of theory, and defined in atomic energy units (Hartree). The energy gap decreases from 0.498 au to 0.388 au for $B_{60}F_{30}H_{30}$, from 0.438 au to 0.372 au for $B_{60}F_{60}$, from 0.433 au to 0.342 au for $B_{60}H_{60}$, and from 0.301 au to 0.258 au for C_{60} with increasing basis set size, being the energy gap of the C_{60} polyhedron the smaller one. Hence, the larger the basis set the smaller the gap. The highest-occupied molecular orbital (HOMO), whose degeneracy is $n_H = 5$, belongs to the H_u irreducible representation for C_{60}, $B_{60}H_{60}$ and $B_{60}F_{30}H_{30}$ molecules. In the $B_{60}F_{60}$ polyhedron, the HOMO belongs to the G_G irreducible representation with degeneracy $n_G = 4$. The lowest-unoccupied molecular orbital (LUMO), whose degeneracy is $n_T = 3$, belong to the T_{2u} and T_{1u} irreducible representations for the compounds $B_{60}H_{60}$ and C_{60} respectively. We should emphasize that in $B_{60}F_{30}H_{30}$, with the basis set where frontier orbitals are shown, 6-31G, the LUMO has T_{2u} symmetry. However, in the cc-pVTZ basis set, this LUMO has A_g symmetry, and the LUMO+1 (which differs by milliHartree from the LUMO) has a T_{2u} symmetry. In other words, the HOMO, LUMO and orbitals just above and below them are very close to each other in energy for $B_{60}H_{60}$, $B_{60}F_{30}H_{30}$ and $B_{60}F_{60}$, as compared to C_{60}. In $B_{60}F_{60}$, the LUMO, LUMO+1, … orbitals are more separatared as compared to $B_{60}H_{60}$ and

Preprints (www.preprints.org) | NOT PEER-REVIEWED | Posted: 13 April 2022 doi:10.20944/preprints202204.0115.v1

$B_{60}F_{30}H_{30}$ and therefore a $B_{60}F_{60}^{(-)}$ monoanion might be considered as a stable species. The isosurfaces of frontier molecular orbitals are shown in Figures 8, 9, 10 and 11 for C_{60}, $B_{60}H_{60}$, $B_{60}F_{30}H_{30}$, and $B_{60}F_{60}$ respectively.

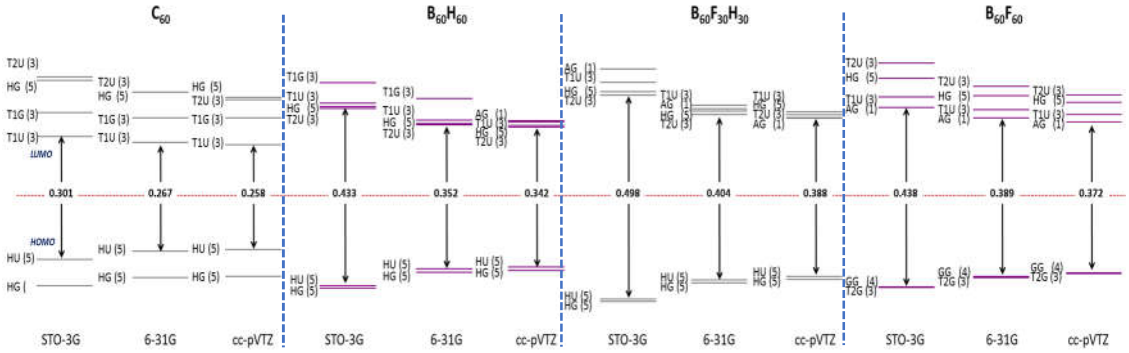

Figure 7. Orbital energy levels of C_{60}, $B_{60}H_{60}$, $B_{60}F_{30}H_{30}$ and $B_{60}F_{60}$. HOMO-LUMO gaps in atomic units E_h (Hartree). RHF computations with the STO-3G, 6-31G and cc-pVTZ basis sets.

The topology of HOMO vs. LUMO changes in all systems, as opposed to C_{60}, since there is no π nodal surface for the HOMOs in the boro(hydride)-fullerenes, namely, the HOMO nature changes in all $B_{60}H_{60}$, $B_{60}H_{30}F_{30}$ and $B_{60}F_{60}$ systems, being an analogous situation with the HOMO/LUMO shapes in diborane(6) ($\pi_{\perp}$ and π^*), as shown in Figure S3 of the SI file. In ethylene, the HOMO and LUMO correspond to the π and π^* molecular orbitals, and thus, the nodal spherical surface applies for the h_u 5-fold degenerate HOMO and the t_{1u} 3-fold degenerate LUMO orbitals, as shown in Figure 8 below.

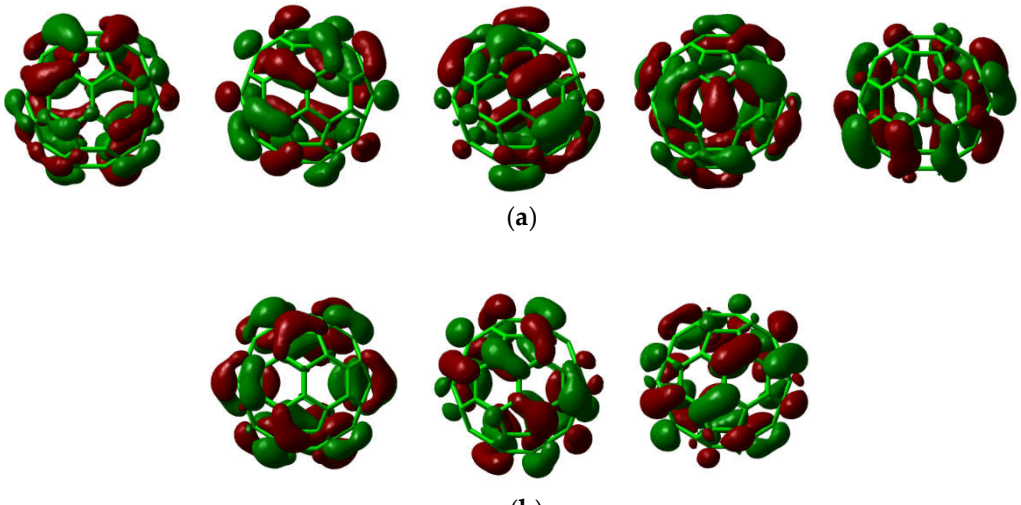

(**a**)

(**b**)

Figure 8. Isosurfaces of frontier molecular orbitals (|0.02| $(e/Bohr^3)^{1/2}$) for the C_{60} molecule using the RHF/6-31G level of theory. Orbital wave-function positive values are indicated in red and negative values in green. (a) HOMO: five degenerate h_u orbitals, b) LUMO: three degenerate t_{1u} orbitals.

Preprints (www.preprints.org) | NOT PEER-REVIEWED | Posted: 13 April 2022 doi:10.20944/preprints202204.0115.v1

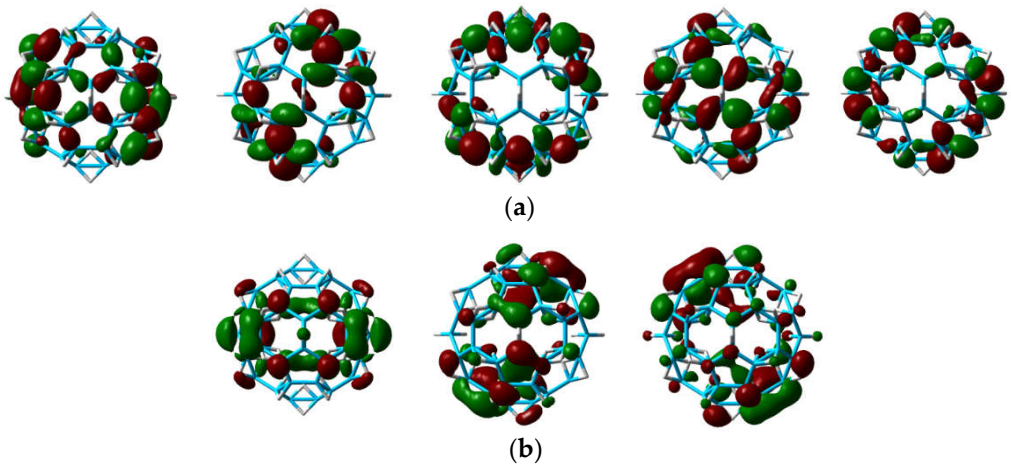

Figure 9. Isosurfaces of frontier molecular orbitals (|0.02| (e/Bohr^3)$^{1/2}$) for the $B_{60}H_{60}$ molecule using the RHF/6-31G level of theory. Orbital wave-function positive values are indicated in red and negative values in green. (a) HOMO: five degenerate h_u orbitals, b) LUMO: three degenerate t_{2u} orbitals.

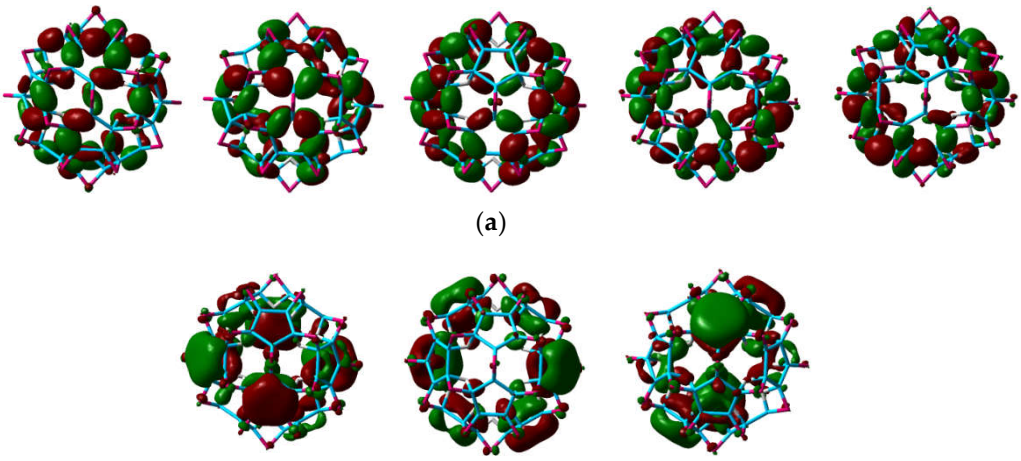

Figure 10. Isosurfaces of frontier molecular orbitals (|0.02| (e/Bohr^3)$^{1/2}$) for the $B_{60}F_{30}H_{30}$ molecule using the RHF/6-31G level of theory. Orbital wave-function positive values are indicated in red and negative values in green. (a) HOMO: five degenerate h_u orbitals, b) LUMO: three degenerate t_{2u} orbitals.

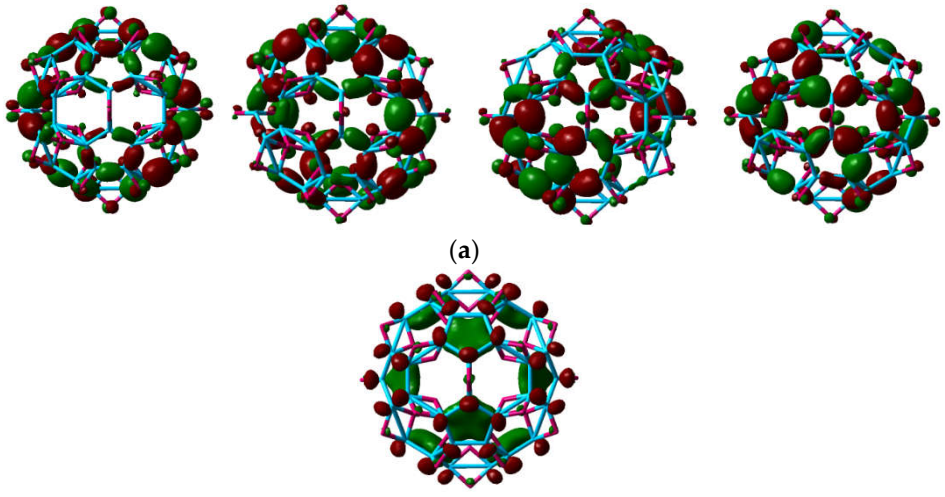

Preprints (www.preprints.org) | NOT PEER-REVIEWED | Posted: 13 April 2022 doi:10.20944/preprints202204.0115.v1

Figure 11. Isosurfaces of frontier molecular orbitals ($|0.02|$ $(e/Bohr^3)^{1/2}$) for the $B_{60}F_{60}$ molecule using the RHF/6-31G level of theory. Orbital wave-function positive values are indicated in red and negative values in green. (a) HOMO: four degenerate g_g orbitals, b) LUMO: one a_g orbital.

As shown in Figures 9, 10 and 11, the HOMO orbitals in the boro-fullerenes have no longer the B_{60} framework as a nodal surface, as explained above. The most significant change of frontier orbital nature is the case of $B_{60}F_{60}$, with a four-fold degenerate G_g HOMO and surprisingly a monodegenerate A_g LUMO. As shown in Figure 11, this LUMO has significant wave-function amplitude inside the B_{60} cage and therefore an anion or electron can be located inside this molecule.

A Hückeloid model [28] was recently introduced to describe π-electron levels of planar borane systems, following the above-mentioned isostructural transformation $C_nH_m \leftrightarrow B_nH_{m+n}$, where C_nH_m is a conjugated hydrocarbon. The parameters of this model are (i) t : electron-transfer parameter between any two adjacent $2p_z$(B) orbitals, similar to the Hückel β parameter (ii) t_b: electron-transfer parameter between a $2p_z$(B) orbital and an adjacent π-$\sigma_u(H_b)_2$ orbital, and (iii) ε_b: the energy of the π-$\sigma_u(H_b)_2$ orbital on the $(H_b)_2$ bridge relative to the $2p_z$(B). According to this model, the π-Hamiltonian is

$$H_{\mathrm{B(K(S))}} = t\sum_{a\sim b}^{\mathrm{S}} T_{a,b} + t_b \sum_{\{a,b\}}^{\pi-\mathrm{K(S)}} \left(T_{ab,a} + T_{ab,b}\right) + \varepsilon_b \sum_{\{a,b\}}^{\pi-\mathrm{K(S)}} T_{ab,ab} \qquad (5)$$

where a and b stand for B atoms and ab means a H_2 π-orbital midway between two boron atoms a and b, K(S) represents a Kekulé structure and B(K(S)) its boronated transformation. A comprehensive description of this model can be found in Ref [28].

We extend this model here to a non-planar system and the above transformation with $n = 60$ and $m = 0$, leading to $B_{60}H_{60}$. In this case, the resolution of the problem within this model implies a 90×90 matrix defined by sixty B atoms and thirty H_2 (elongated) molecules. Note that the Hückel model forms a 60×60 matrix from sixty C atoms. In order to compare the Hückeloid model spectrum with the RHF π-energy levels, we consider five energy levels below the HOMO and five energy levels above the LUMO. In the Supplementary Information we describe the calculation of the RHF π-energy orbital levels. Each energy level in Figure 12 and Figure 13 below is shifted so that the zero Fermi-level is midway between the HOMO and LUMO, within a T = 0 K approximation. Furthermore, the orbital π-energy levels of ab initio results are multiplied by a factor f in order to match the HOMO–LUMO gap for the exact Hückeloid model with parameters $t = -1$, $t_b = 2t$ and $\varepsilon_b = -0.2|t|$. Comparison between the Hückeloid and Hückel models with their respective ab-initio calculations shows that the Hückeloid model is closer to its respective ab-initio orbital energies, as depicted in Figure 12 and Figure 13. We should emphasize that n the Hückel model there is an accidental degeneracy in the LUMO+2 level, while in the Hückeloid model the symmetries of HOMO-2 and HOMO-3 are exchanged thus presenting 3- and 4- degeneracies, instead of 4- and 3-degeneracies, as in the SCF computation.

Preprints (www.preprints.org) | NOT PEER-REVIEWED | Posted: 13 April 2022 doi:10.20944/preprints202204.0115.v1

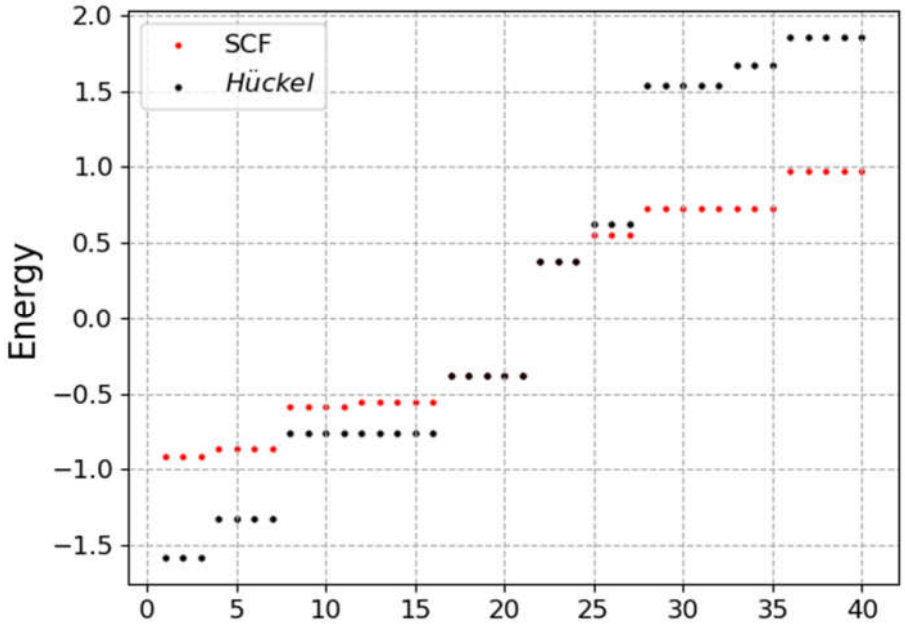

Figure 12. C_{60}: π-orbital energy levels of the Hückel model and ab initio SCF computation, scaled with a factor *f* in order to match the HOMO–LUMO gap for this model. The values in red correspond to the RHF/6-31G computations.

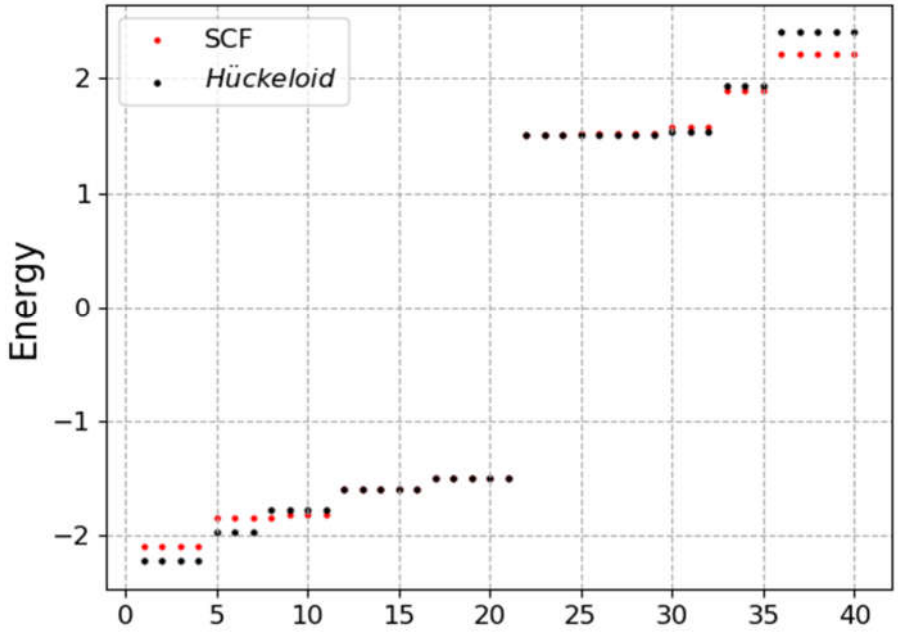

Figure 13. $B_{60}H_{60}$: π-orbital energy levels of the Hückeloid model and ab initio SCF computation, scaled with a factor *f* in order to match the HOMO–LUMO gap for this model. The values in red correspond to the RHF/6-31G computations. Exact solution of Hückeloid model with $t = -1$, $t_b = 2t$ and $\varepsilon_b = -0.2|t|$.

2.4. Electronic structure: Topological properties of the electron density

2.4.1. Quantum theory of atoms-in-molecules

The topological properties of the electron density $\rho(\boldsymbol{r})$ – the latter an observable – can give important chemical insight. Thus, according to QTAIM, the molecular structure in a given system is revealed by the stationary (critical) points ($\vec{\nabla}\rho = \vec{0}$) of the electron density

Preprints (www.preprints.org) | NOT PEER-REVIEWED | Posted: 13 April 2022 doi:10.20944/preprints202204.0115.v1

gradient together with the gradient paths of the electron density that originate and terminate at these points [29,30]. In this theory, we take the Laplacian of the density $(\nabla^2\rho)_{ij}$ at critical points and diagonalize this (3×3) matrix and analyze the sign of the eigenvalues (λ_1, λ_2, λ_3), provided all eigenvalues are not zero. Thus, we classify the critical points with the (n, s_n) pairs, where n is the number of non-zero eigenvalues of the Laplacian and s_n is the sum of the signs of these eigenvalues. Thus, the pairs (3, -3) correspond to nuclei positions; (3, -1) are bond critical points (BCP); (3, +1) ring critical points (RCP) and (3,+3) cage critical points. For bond critical points, $\lambda_3 > 0$ is associated with the bond path direction, and $\lambda_1 < 0$, $\lambda_2 < 0$ associated with the two directions where $\nabla^2\rho$ is a maximum.

Application of QTAIM to the systems included in this work results on the molecular graphs depicted in Figure 14 and the values of the electron density $\rho(r)$ and its Laplacian $\nabla^2\rho$ in all symmetry-unique bond and ring critical points, gathered in Table 3.

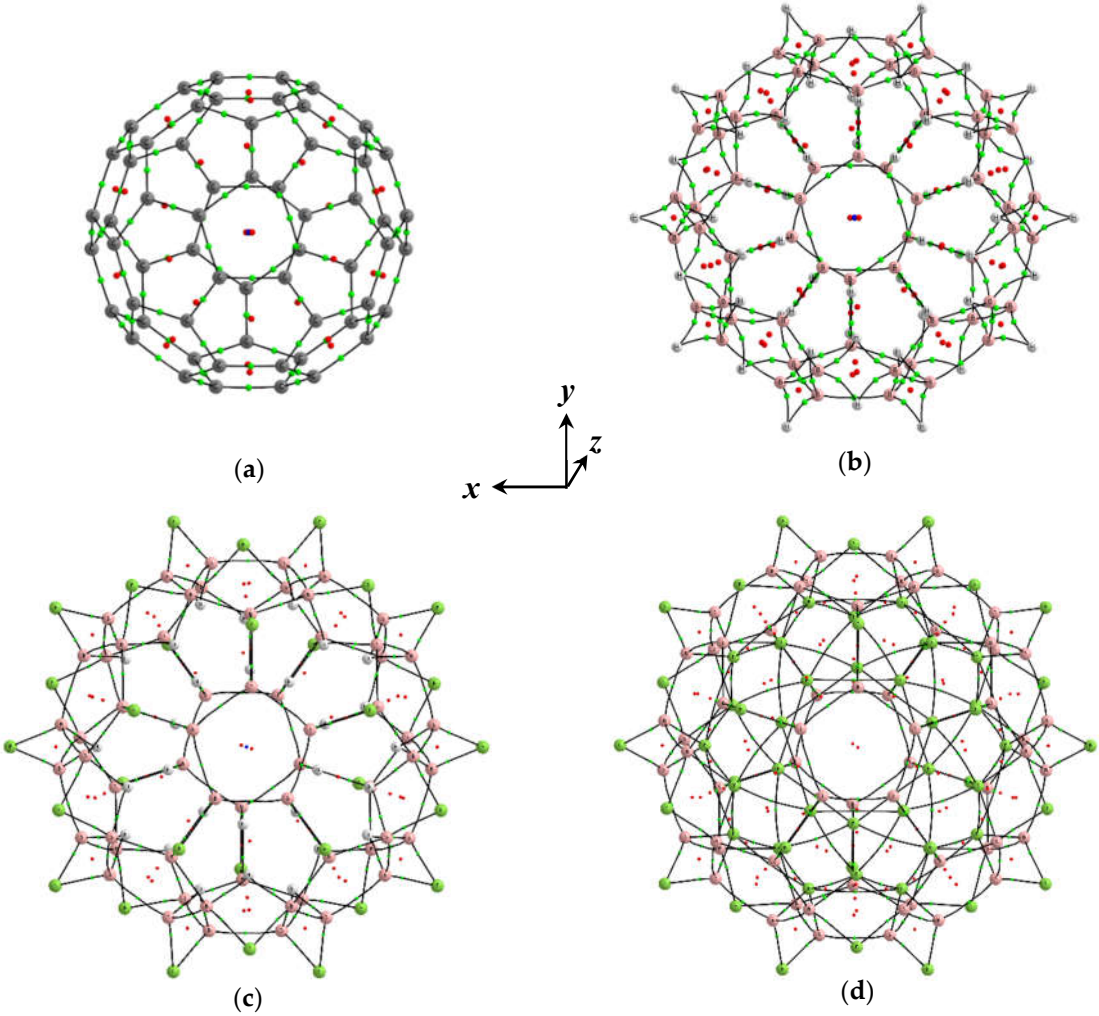

Figure 14. Molecular graph in (a) C_{60} , (b) $B_{60}H_{60}$, (c) $B_{60}F_{30}H_{30}$ and (d) $B_{60}F_{60}$, with bond paths (black lines), bond (green), ring (red) and cage (blue) critical points of the electron density. The graphs are displayed with a 3º rotation around the y axis in order to see the cage critical point (blue) at the center of the cage for C_{60}, $B_{60}H_{60}$ and $B_{60}F_{30}H_{30}$, but absent in $B_{60}F_{60}$. B3LYP/cc-pVDZ computations.

Preprints (www.preprints.org) | NOT PEER-REVIEWED | Posted: 13 April 2022 doi:10.20944/preprints202204.0115.v1

Table 3. Values of the electron density ρ (e/a_0^3) and its Laplacian $\nabla^2\rho$ (e/a_0^5) at the symmetry-unique bond (BCP, green) and ring (RCP, red) critical points for C_{60}, $B_{60}H_{60}$, $B_{60}F_{30}H_{30}$ and $B_{60}F_{60}$.

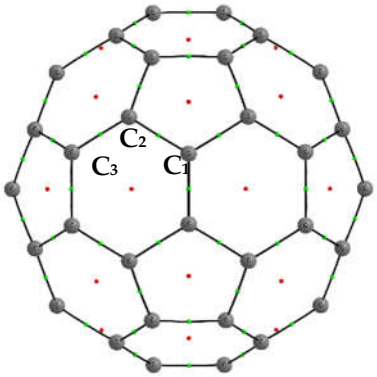

C_{60}	moiety	ρ	$\nabla^2\rho$
BCP_1	C1-C2	0.274767	-0.610460
BCP_2	C2-C3	0.302503	-0.712539
RCP_1	pentagon	0.043831	+0.299022
RCP_2	hexagon	0.019890	+0.148725

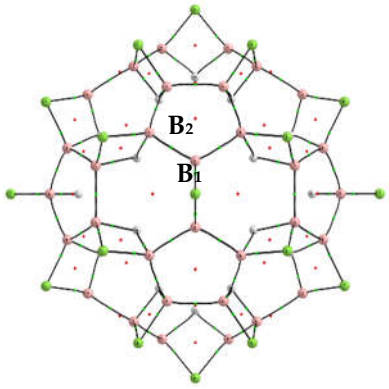

$B_{60}F_{30}H_{30}$	moiety	ρ	$\nabla^2\rho$
BCP_1	B1-B2	0.150492	-0.300721
BCP_2	B-H	0.107392	+0.135730
BCP_3	B-F	0.090437	+0.485301
RCP_1	$B(F_{out}H_{in})B$	0.073035	+0.147444
RCP_2	B_5	0.023860	+0.089056
RCP_3	$B_6(H_{in})_3$	0.007312	+0.042445

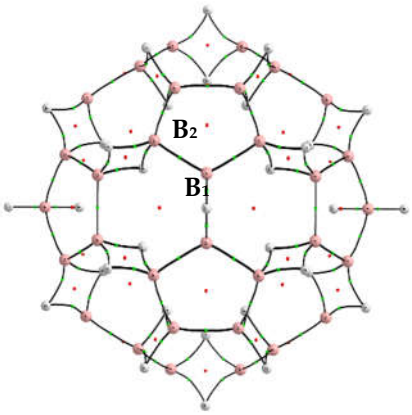

$B_{60}H_{60}$	moiety	ρ	$\nabla^2\rho$
BCP_1	B1-B2	0.143063	-0.269949
BCP_2	$B\text{-}H_{in}$	0.114026	+0.192718
BCP_3	$B\text{-}H_{out}$	0.108905	+0.069211
RCP_1	$B(H_2)B$	0.100256	+0.021501
RCP_2	B_5	0.023765	+0.088674
RCP_3	$B_6H_{3(in)}$	0.009156	+0.054290

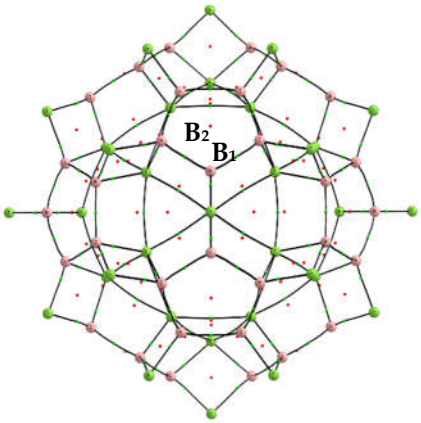

$B_{60}F_{60}$	moiety	ρ	$\nabla^2\rho$
BCP_1	B1-B2	0.147043	-0.292392
BCP_2	$B1\text{-}F_{in}$	0.091620	+0.473343
BCP_3	$B1\text{-}F_{out}$	0.082091	+0.312053
BCP_4	$F_{in}\text{-}F_{in}'$	0.025007	+0.127742
RCP_1	B_5	0.020617	+0.079982
RCP_2	$B(F_2)B$	0.058252	+0.284142
RCP_3*	$B_2(F_{in})_2$	0.024664	+0.123339
RCP_4	$(F_{in})_3$	0.014346	+0.076786

* Very close to BCP_4

As shown in Figure 14 and Table 3, two symmetry-unique BCP appear in C_{60}, in the C1C2 and C2C3 connections, with a larger value of ρ for the C2C3 bond joining two hexagons. The negative values of the Laplacian in these BCP show charge cummulations at these points. In $B_{60}H_{60}$, four BCP appear in the $B2(H_{in}H_{out})B3$ rhombus, for each B-H con-

Preprints (www.preprints.org) | NOT PEER-REVIEWED | Posted: 13 April 2022 doi:10.20944/preprints202204.0115.v1

nection, and a central RCP. The Laplacian values for the B-H bonds are positive, an indication of charge depletion. As in C_{60}, in $B_{60}H_{60}$ there is a RCP at the center of each pentagon and hexagon. This also holds for $B_{60}F_{30}H_{30}$ and $B_{60}F_{60}$. For the $B_{60}F_{30}H_{30}$ molecule, there are the same number of BCP and RCP as compared to $B_{60}H_{60}$. Again, the B-H interactions have positive values of the Laplacian, and so have the B-F interactions, with the BCP very close to the B atom. The B1-B2 interaction in $B_{60}F_{30}H_{30}$ is still of covalent nature with a ρ_{BCP} = 0.1505, slightly larger as compared to $B_{60}H_{60}$. Finally, the topological properties of $B_{60}F_{60}$ are quite peculiar due to the inner F atom network [31,32] connected through bond paths; we have then expected three BCP: B1-B2, B-F_{in} and B-F_{out}, all with positive Laplacian and thus all electron density depletion points. However, due to the close contacts between the F_{in} neighbor atoms (2.341 Å; in the F_2 molecule, experimental *d*(FF) = 1.412 Å [33]), these are connected to each other through a bond path. A comparison between Figure 14d and the $B_{60}F_{60}$ molecule in Table 3 can give an insight of this F atom pattern, also with I_h icosahedral symmetry, and displayed in Figure 15.

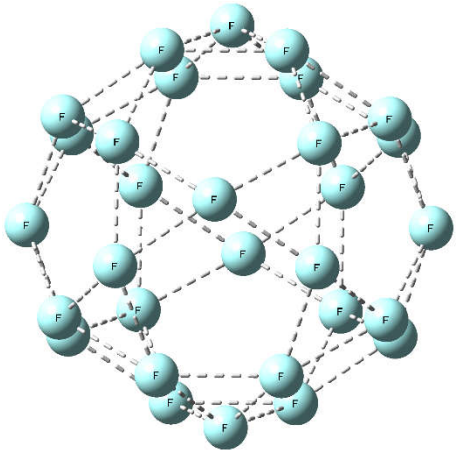

Figure 15. The icosahedral I_h pattern for the thirty F_{in} atoms in $B_{60}F_{60}$. There is a bond critical point at the mid point between any two neighbor F atoms – d(FF) = 2.341 Å – and a ring critical point at the center of each triangle and pentagon. In F_2, the experimental distance d(FF) is 1.412 Å [33]. See also Figure 14d and Table 3.

2.4.2. Electron Localization function

A further tool to analyze with the topological properties of the electron density is the Electron Localization Function (ELF). This function gives a measure of the likelihood of finding an electron in the neighborhood space of a reference electron located at a given point and with the same spin. The ELF gives the extent of spatial localization of the reference electron with a mapping of electron pair probability in multielectronic systems [34,35], and divides the molecular space into regions, called basins. These basins have a non-negligible probability of containing a pair of electrons. Depending on the number of nuclei involved and the type of electrons, the basins are labeled as: Core C(A), Monosynaptic V(A), Disynaptic V(A, X), etc. The ELF function for all the systems included in this work is depicted in Figure 16 by space-distribution through chemical-bonds, in different cross-sectional planes. As shown in Figures 16a and 16b, in C_{60} there are two different disynaptic basins, namely V(C1, C2) = 2.4 and V(C2,C3) = 3.0, corresponding respectively to the CC bond in pentagonal and hexagonal moieties. As for $B_{60}H_{60}$, there are three cross-sectional planes, apart from the pentagonal and hexagonal moieties, due to the B(H_2)B rhombus moiety shown in Figure 16c, with two trisynaptic basins V(B,B,H_{in}) and V(B,B,H_{out}) with a respective population of 1.84 and 1.94 electrons. The pentagonal moiety in $B_{60}H_{60}$ has a disynaptic basin V(B,B), containing a very localized pair of electrons (the value of the ELF is close to 1.0 and the population is larger than 2.0 electrons), as shown in Figures 16d and 16e. The number of electrons in those basins is lower than in V(C1,C2)

Preprints (www.preprints.org) | NOT PEER-REVIEWED | Posted: 13 April 2022 doi:10.20944/preprints202204.0115.v1

of C_{60}, but the electrons are more localized: the value of the ELF is close to 1.0 for $B_{60}H_{60}$ and 0.90 for C_{60}.

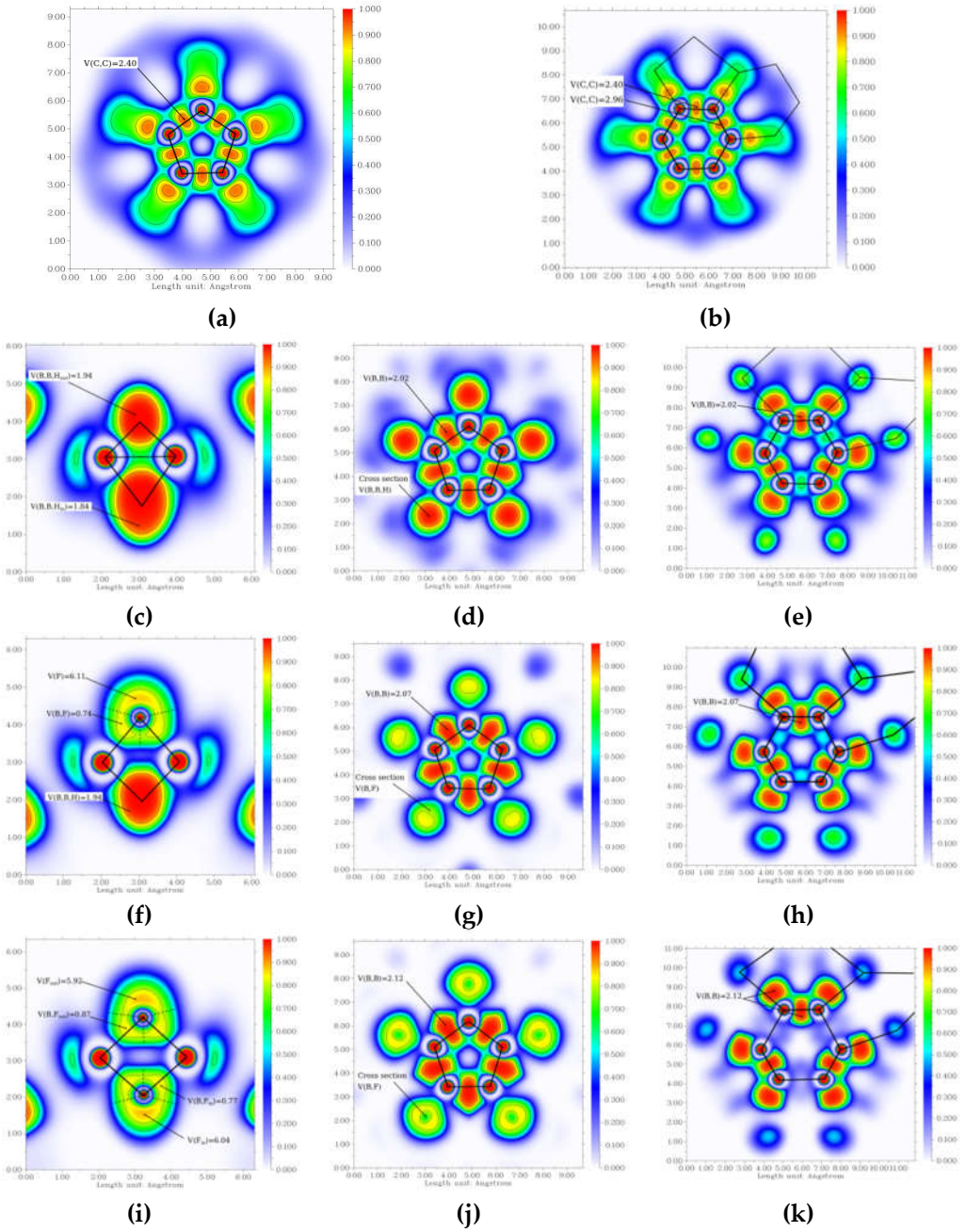

Figure 16. ELF function projected on different cross-sectional planes: (a) C_{60} pentagons, (b) C_{60} hexagons, (c) $B(H_2)B$ moiety plane in $B_{60}H_{60}$, (d) pentagons in $B_{60}H_{60}$, (e) hexagons in $B_{60}H_{60}$, (f) $B(F_{out})(H_{in})B$ moiety plane in $B_{60}F_{30}H_{30}$, (g) pentagons in $B_{60}F_{30}H_{30}$, (h) hexagons in $B_{60}F_{30}H_{30}$, (i) $B(F_2)B$ moiety plane in $B_{60}F_{60}$, (j) pentagons in $B_{60}F_{60}$, (k) hexagons in $B_{60}F_{60}$.

The three cross-sectional ELF pictures of the $B_{60}F_{30}H_{30}$ molecule are depicted in Figures 16f, 16g and 16h, with the rhombus $B(F_{out}H_{in})B$, the pentagonal and hexagonal moieties respectively. The B-F_{out}-B connectivity can be described by two disynaptic basins $V(B,F_{out})$, with a population of 0.87 electrons and an ELF value around 0.85. The 6.11 electrons of the fluorine lone pair, $V(F_{out})$, are slightly more localized than in the $V(B,F_{out})$ basins. The B-H-B link is very similar to the $V(B,B,H_{out})$ observed in $B_{60}H_{60}$, namely very localized and with a population of around 1.9 electrons. Finally, we collected the ELF plots for $B_{60}F_{60}$ in Figure 16i, 16j, 16k. In $B_{60}F_{60}$, the B-$F_{in/out}$-B link is similar to the B-F-B bond in $B_{60}F_{30}H_{30}$, with the F_{in} less bonded to the boron atoms than F_{out}: the number of electrons in

Preprints (www.preprints.org) | NOT PEER-REVIEWED | Posted: 13 April 2022 doi:10.20944/preprints202204.0115.v1

the V(B,B,F_{in}) is lower, the ELF value of those basins is bit a lower, the lone pair of the fluorine, V(F_{in}), contains more electrons. The V(B,B) basins contain 2.12 electrons, with the highest V(B,B) population among the three boron compounds.

2.5. Stability of neutral closo-boranes: $B_{16}H_{16}$, $B_{19}H_{19}$, $B_{22}H_{22}$, and $B_{60}H_{60}$.

The energy per BH unit is generally considered a measure of the relative stability of the *closo*-boranes B_nH_n . We computed the energy per BH unit of $B_{60}H_{60}$ and compared it to previously reported smaller neutral *closo*-boranes $B_{16}H_{16}$ (T_d), $B_{19}H_{19}$ (C_{3v}) and $B_{22}H_{22}$ (T_d) [36]; the optimized geometries and structures of these molecules are included in the SI file.

Table 4. The energy per BH unit – {E/*n*(BH)} (au) - and the relative values – {E/*n*(BH)}$_{rel}$ (kJ·mol^{-1}) - in $B_{60}H_{60}$ (I_h), and previously reported [36] *closo*-boranes $B_{16}H_{16}$ (T_d), $B_{19}H_{19}$ (C_{3v}) and $B_{22}H_{22}$ (T_d), computed at DLPNO/CCSD(T)/def2-SVP and B3LYP/cc-pVDZ levels of theory.

Method →	**DLPNO**	**DLPNO**	**B3LYP**	**B3LYP**	**Ref [36]**	**Ref [36]**
System	E/*n*(BH)	{E/*n*(BH)}$_{rel}$	E/*n*(BH)	{E/*n*(BH)}$_{rel}$	E/*n*(BH)	{E/*n*(BH)}$_{rel}$
$B_{16}H_{16}$ (T_d)	-25.35485	0.0	-25.45908	0.0	-25.244	13.1
$B_{19}H_{19}$ (C_{3v})	-25.35378	2.8	-25.45793	3.0	-25.243	15.8
$B_{22}H_{22}$ (T_d)	-25.35448	1.0	-25.45830	2.0	-25.249	0.0
$B_{60}H_{60}$ (I_h)	-25.32711	72.8	-25.43230	70.3	---	---

As shown in Table 4, previous reported values give $B_{22}H_{22}$ a larger stability as compared to $B_{16}H_{16}$ and $B_{19}H_{19}$. This is contrast with our computations, where $B_{16}H_{16}$ is more stable than the larger *closo*-boranes and indeed more stable than $B_{60}H_{60}$; however, we should take into account that the previous computations where carried out with less accurate methods and with computational resources which cannot be compared to current resources. Our computed relative energies per BH unit are very small when comparing $B_{16}H_{16}$ with $B_{19}H_{19}$ and $B_{22}H_{22}$, but large when compared to $B_{60}H_{60}$; hence, the smaller *closo*-boranes should be more stable, according to energies per BH unit.

On the other hand, the binding energy that can ensure the stability of a system can be calculated using the following formula [37]

$$\frac{E_{BE}}{N} = \frac{N_B}{N} E_B + \frac{N_H}{N} E_H - \frac{E_T}{N} \qquad (6)$$

where N_X and E_X are the number of X forming atoms and its energy respectively and E_T is the total energy, with $N = N_B + N_H$. This magnitude can be considered as the energy released when forming a system when bringing all B and H atoms from infinite to the considered energy minimum geometry. Thus, the more positive the binding energy the more stable the system. In Table 5 these binding energies are gathered for the same set of neutral *closo*-boranes as considered above.

Table 5. Binding energies, according to Eq.(6) for neutral closo-boranes. E_{BE} and E_{BE}/N in a.u. (Hartree) and relative binding energies Δ(E_{BE}/N) in kJ·mol^{-1}. Quantum-chemical computations with the B3LYP/cc-pVDZ and DLPNO/TZVP models.

	B3LYP/cc-pVDZ			DLPNO/TZVP		
System	E_{BE}	E_{BE}/N	Δ(E_{BE}/N)	E_{BE} (au)	E_{BE}/N	Δ(E_{BE}/N)
$B_{16}H_{16}$	4.75118	0.14847	0.0	4.76591	0.14893	0.0
$B_{19}H_{19}$	5.62018	0.14790	-1.5	5.63973	0.14841	-1.4
$B_{22}H_{22}$	6.51572	0.14808	-1.0	6.54626	0.14878	-0.4
$B_{60}H_{60}$	16.21014	0.13508	-35.2	16.19836	0.13499	-36.6

As shown in Table 5, the binding energy follows the same relative order as compared to the energy per BH unit, as described above. The most stable system is again $B_{16}H_{16}$,

Preprints (www.preprints.org) | NOT PEER-REVIEWED | Posted: 13 April 2022 doi:10.20944/preprints202204.0115.v1

followed very close in energy by $B_{22}H_{22}$ and $B_{19}H_{19}$, with the $B_{60}H_{60}$ relative binding energy 37 kJ·mol^{-1} lower.

2.6. Heats of formation

Finally, computed thermochemical data are included in order to give some hints for potential syntheses of these molecules. The heat of formation for $B_{60}H_{60}$ [38], $B_{60}F_{30}H_{30}$ and $B_{60}F_{60}$ is reported by means of the experimental heats of formation [39] of hydrogen, boron and fluorine: 218 kJ·mol^{-1}, 560 kJ·mol^{-1} and 79 kJ·mol^{-1}, respectively, and the quantum-chemical computations of enthalpy at standard conditions (T = 298 K and P = 1 bar), according to the following reactions:

$$B_{60}H_{60}(g) \rightarrow 60B(g) + 60H(g) \quad (7)$$

$$B_{60}F_{30}H_{30}(g) \rightarrow 60B(g) + 30F(g) + 30H(g) \quad (8)$$

$$B_{60}F_{60}(g) \rightarrow 60B(g) + 60F(g) \quad (9)$$

The enthalpy of reaction (7), (8) and (9) at standard conditions corresponds to the heat of formation for each compound. Thus, combining the experimental heats of formation of hydrogen, boron and fluorine with the computed enthalpies in (7), (8) and (9), one can obtain the computed heats of formation $\Delta H_f^0(g)$, as gathered in Table 6.

Table 6. Computed heats of formation $\Delta H_f^0(g)$ for $B_{60}H_{60}$, $B_{60}F_{30}H_{30}$ and $B_{60}F_{60}$ in kJ·mol^{-1}. Enthalpy H (au) quantum-chemical computations with the B3LYP/cc-pVDZ model. Experimental heats of formation for H, B and F from Ref [39].

	H(au)	$\Delta H_f^0(g)$
H	-0.498897[b]	218[a]
B	-24.658513[b]	560[a]
F	-99.724241[b]	79[a]
$B_{60}H_{60}$	-1525.054532[b]	5696[b]
$B_{60}F_{30}H_{30}$	-4503.824528[b]	3750[b]
$B_{60}F_{60}$	-7482.261227[b]	12322[b]

a. Experimental values from Ref [39].
b. B3LYP/cc-pVDZ computations.

According to our computations, the lowest heat of formation corresponds to $B_{60}F_{30}H_{30}$, followed by $B_{60}H_{60}$ and $B_{60}F_{60}$, the latter being considerably larger, possibly due to the F···F interactions inside the B_{60} cage. We have included the heat of formation of C_{60} for comparative purposes and it turns out to be lower than in $B_{60}H_{60}$ and similar as compared to $B_{60}F_{30}H_{30}$.

3. Discussion

The chemistries of boron and carbon are very different: the four valence electrons $2s^2 2p^2$ in carbon can be distributed into 3D structures like diamond, 2D structures like graphene and 1D structures like polyacetylene. The discovery of Buckminsterfullerene C_{60} in 1985 [12] opened the door to novel phases of carbon, followed by carbon nanotubes [40], i.e., folded graphene with different cuts into cylindrical shapes with different symmetry. On the other hand and within the chemistry of boron, the early XXth century pioneering work of Stock on boranes or boron hydrides B_nH_m [41] led to a major interest for these polyhedral compounds, truncated (open) or closed (*closo*) B_nH_m polyhedra. Boron atoms in boranes tend to clusterize because boron has only three valence electrons $2s^2 2p^1$ and addition of hydrogens (an additional electron) helps in the stabilization of the structures. The different atomic 1*s*, 2*s* and 2*p* energy levels in boron and carbon are also responsible for these different molecular architectures. We should emphasize that boron does

Preprints (www.preprints.org) | NOT PEER-REVIEWED | Posted: 13 April 2022 doi:10.20944/preprints202204.0115.v1

not follow the octet rule [42], and forms multicentric bonds [43,44]. The pioneering work of Lipscomb *et al* in the decades 1960s-1970s helped in the understanding of the 3D structural elucidation of boranes [45].

In an attempt to relate boron and carbon 2D chemistries, a recent experimental finding calls for a potential new 2D boron chemistry: the isolation from the superconductor MgB_2 of a borophane 2D layer $(BH)_1$ isostructural and isoelectronic with graphene [46]. Previous theoretical works on the prediction of planarity in boron molecules and boron compounds have been published [1,6,10,11,47]. The simple link between hydrocarbon and borane chemistries [5] can be applied to conjugated hydrocarbons C_nH_m and the corresponding boranes B_nH_{m+n} [10,11]. If we set m = 0, the transformation $C_n \rightarrow B_nH_n$ can be established. Without any doubt the most popular conjugated C_n structure is Buckminsterfullerene C_{60} , and the corresponding borane is $B_{60}H_{60}$, also with icosahedral symmetry and the same number of electrons. The presence of H_{in} and H_{out} symmetry-different bridging hydrogen atoms in $B_{60}H_{60}$ – see Figure 1b and Table 1 – allows for substitutions where the icosahedral symmetry is maintained. Thus, we substituted all H_{in} and/or H_{out} atoms by monovalent fluorine atoms, thus obtaining the structures shown in Figure 1c, Figure 1d and Figure 1e: $B_{60}(F_{30})_{out}(H_{30})_{in}$, $B_{60}(F_{30})_{in}(H_{30})_{out}$ and $B_{60}F_{60}$ respectively. It turns out that a geometry optimization of all structures led to energy minima, except for the $B_{60}(F_{30})_{in}(H_{30})_{out}$ structure – Figure 1d – whose optimization leads to an icosahedral stationary point with seven imaginary frequencies. Removal of the first imaginary frequency led to a collapsed structure, as shown in Figure 16 below.

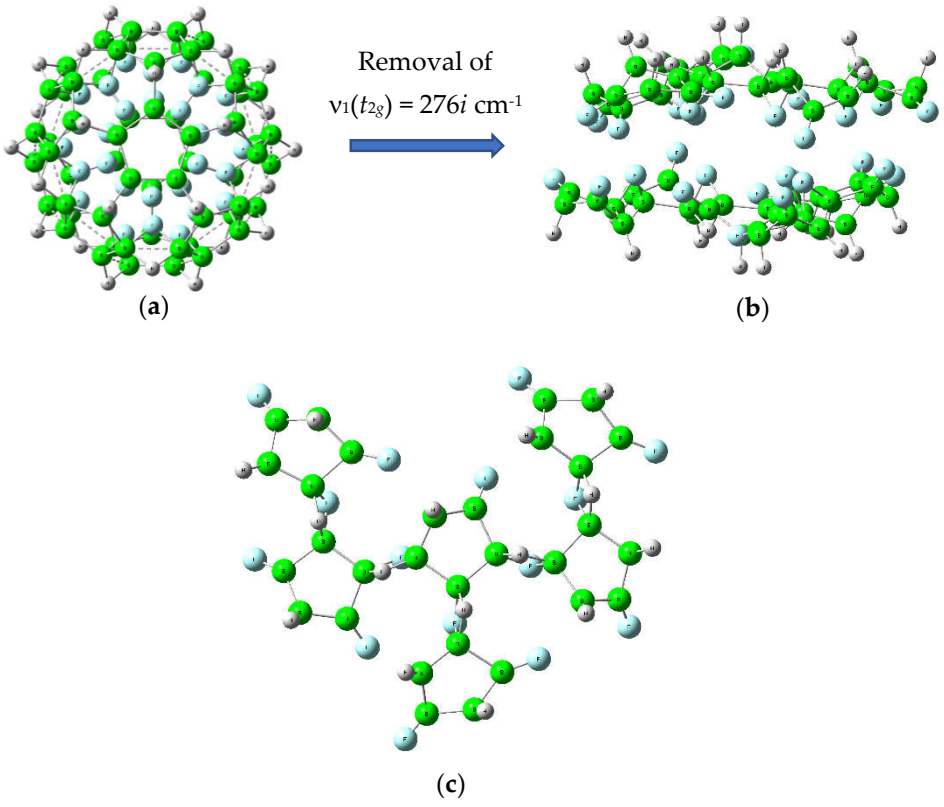

Figure 16. (a) Removal of the first imaginary frequency $\nu_1(t_{2g}) = 276i$ cm^{-1} in the 7th – order saddle point structure $B_{60}(F_{30})_{in}(H_{30})_{out}$ with icosahedral symmetry I_h. (b) Double layer optimized collapsed structure. (c) One layer of the collapsed structure projected on the screen plane: Distorted boron pentagons bonded through $B(F)_{in}(H)_{out}B$ moieties.

In Buckminsterfullerene, the experimental C_1C_2 (pentagonal) and C_2C_3 (hexagonal) bond distances are 1.45 Å and 1.40 Å respectively [48]. As gathered in Table 1, the B3LYP/cc-pVDZ computed distances are 1.46 Å and 1.40 Å, *i.e.* in very good agreement with the experimental distances. The shorter distance C_2C_3 is the same as in benzene. The transformation $C_{60} \rightarrow B_{60}H_{60}$ leads to the structure shown in Figure 1b with geometrical

Preprints (www.preprints.org) | NOT PEER-REVIEWED | Posted: 13 April 2022 doi:10.20944/preprints202204.0115.v1

data in Table 1. We will focus on the BB distances in $B_{60}H_{60}$: there are two of them, as in C_{60}. The short "direct" B_1B_2 bonds with 1.75 Å and forming the pentagons and the long B_2B_3 = $B(H_2)B$ = 1.87 Å distances with alternation in the hexagonal moieties. The experimental $B(H_2)B$ distance in diborane(6) is 1.74 Å [49], which is similar to the "direct" B_1B_2 bond in $B_{60}H_{60}$, but should correspond structurally to B_2B_3 = 1.87 Å; hence the $B_{60}H_{60}$ is a sort of swelled concatenation of diborane(6) molecules connecting B_5 pentagons, the whole system resembling C_{60} , but with larger volume and also with icosahedral symmetry. In the case of diborane(4), the BB computed distance is 1.48 Å, and complexes of this molecule are known [50]. As for the hypothetical H-B=B-H molecule [51], the computed BB distance is 1.54 Å, which would be equivalent to the experimental CC bond distance in ethane.

We turn now to the "stable" *i.e.* energy minimum icosahedral structure $B_{60}(F_{30})_{out}(H_{30})_{in}$ – Figure 1c – labeled as $B_{60}F_{30}H_{30}$. The "short" B_1B_2 bond in the B_5 pentagons is very similar, slightly shorter, as compared to $B_{60}H_{60}$. However, for the "long" B_2B_3 distance, the presence of the bridging F_{out} atoms elongates this distance considerably as compared to $B_{60}H_{60}$. The BF_{out} bond distance is longer than in BF_3 [52] since the fluorine atom is shared by two boron atoms. As for the BH_{in} distances, these are slightly longer than in $B_{60}H_{60}$. Finally, in the perfluorinated $B_{60}F_{60}$, given the larger size of fluorine as compared to hydrogen, the B_1B_2 and B_2B_3 distances are 1.781 Å and 2.389 Å respectively, showing a considerable larger elongation for the $B(F_2)B$ distance. Notwithstanding it is a bit surprising that this structure is an energy minimum. The hexafluorodiborane(6) B_2F_6 does not exist as far as we know and a B3LYP/cc-pVDZ geometry optimization with the diborane(6) structure leads to a transition state with an imaginary frequency leading to two BF_3 molecules. A similar situation takes place with the $B_2F_6\cdots BeF_2$ complexes [53]. The BF_{in} bond distance in $B_{60}F_{60}$ is similar as compared to $B_{60}F_{30}H_{30}$, but the BF_{out} distance is slightly elongated, still far from the BF distance in BF_3, the latter being 1.30 Å [52].

The MEP in the four stable systems C_{60}, $B_{60}H_{60}$, $B_{60}F_{30}H_{30}$ and $B_{60}F_{60}$ displayed in Figure 2 show clear different patterns. Thus, negative charge attraction areas – blue color – appear above pentagons and hexagons in C_{60}; however, in $B_{60}H_{60}$ these areas appear only on the BHB moieties from hexagons. These patterns also change in $B_{60}F_{30}H_{30}$ with negative charge attraction areas above pentagons and slight positive charge attraction areas – red color – along the BFB moiety. In $B_{60}F_{60}$ these effects are more pronounced, with very strong negative attraction areas above pentagons, and very strong positive attraction areas along the BFB moiety. The red area inside the 2D slice cut-off in $B_{60}F_{60}$ is a clear indication that a cation, a proton or a positive charged species could be stabilized inside the cluster, provided steric hindrance is avoided.

The charges, bond orders and localized molecular orbitals give a clear picture of the electronic structure differences between the molecules. Thus, the bond orders for the 2c-2e bonds C_1C_2 and C_2C_3 show 1.16 and 1.41 electrons respectively, in agreement with their distances. The fact that the (Pauling) electronegativity order is X(F) = 3.98 >> X(C) = 2.55 > X(H) = 2.20 > X(B) = 2.04, provides basically null charges in $B_{60}H_{60}$, with q(B) = 0.00, $q(H_{in})$ = 0.07, $q(H_{out})$ = -0.08. When substituting H_{out} atoms by fluorine atoms in $B_{60}H_{60}$ the charge on boron changes considerably to q(B) = +0.17, with q(F) = -0.27 and q(H) = -0.06, the latter similar to $q(H_{out})$ in $B_{60}H_{60}$. The positive charges in q(B) are almost doubled in $B_{60}F_{60}$, due to the electronegativity of fluorine. The stability of the $B_{60}F_{60}$ cage is striking, as stated above, due to the non-existence of B_2F_6 and its origin could well be due to $F_{in}\cdots F_{in}$ attraction dispersion forces and a co-operative effect of the B_5 pentagons joined by $B(F_2)B$ moieties. Let us remind that the icosahedral $B_{60}(F_{30})_{in}(H_{30})_{out}$ structure is not an energy minimum but a 7^{th}–order saddle point (Figure 16).

The bond order indices of all systems give a hint on how the electrons are distributed, especially in the multicentric bonds. The three-center two-electron (3c-2e) bonds, 3c : BHB, in B_2H_6 can be easily explained with the $(\sigma + \pi)$ and $(\sigma - \pi)$ combinations of the orthonormal molecular orbitals σ and π, each with two electrons. The positive and negative combinations are the two famous two "banana" bonds that describe the four valence electrons in B_2H_6 which are not involve in the B-H_t 2c-2e bonds, with H_t = terminal hydrogen. Thus,

Preprints (www.preprints.org) | NOT PEER-REVIEWED | Posted: 13 April 2022 doi:10.20944/preprints202204.0115.v1

bond order 2c-2e indices in C1C2 and C2C3 show values of 1.16 and 1.41 for C_{60}. The situation changes drastically in $B_{60}H_{60}$ due to the longer B2B3 distance, as compared to C2C3. However, for B1B2 the 2c-2e bond order is very similar along the $B_{60}H_{60}$, $B_{60}F_{30}H_{30}$ and $B_{60}F_{60}$ molecules, a clear indication that the B_5 pentagons are electronically and structurally (*vide supra*) very similar. However the hexagonal moieties change electronically, as shown by the bond order indices of B2B3, from 0.37 in

$B_{60}H_{60}$ to 0.18 in $B_{60}F_{30}H_{30}$ and basically zero in $B_{60}F_{60}$. The presence of fluorine atoms changes the interactions; thus, the bond order indices 2c-2e' (B_2X_{out}), 2c-2e' (B_2X_{in}), 3c-2e ($B_2X_{in}B_3$) and 3c-2e' ($B_2X_{out}B_3$), with X = {H, F}, give clear pictures of the bonding: In $B_{60}H_{60}$, these values are 0.49, 0.47, 0.24 and 0.20 respectively. Namely, one electron in the B-H_{in} and B-H_{out} and half an electron in the BH_{in}B and BH_{out}B three-center moieties. Substitution of all H_{out} by fluorine atoms leads to a major change in the 3c-2e' (B2FB3) moiety with a basically zero bond order index, with the remaining bond order indices very similar, due to the longer B2B3 distance with the presence of a fluorine atom in between. Finally, in $B_{60}F_{60}$ all 3c-2e bonds have basically zero bond order index, with the 2c-2e ($B2F_{in}$) and ($B2F_{out}$) values close to ½ ; let us recall that the B2B3 and B1B2 bond orders in $B_{60}F_{60}$ are zero and one respectively. Therefore, from the bond orders point of view we can consider these systems as B5 pentagons joined by hexagonal moieties that change electronic structure as function of the presence of fluorine atoms in the alternant bridge BXB positions.

The localized molecular orbitals (LMO) from Figures 3-6 give a complementary picture of the previous discussion. Here each LMO has a population of two electrons: in C60, the σ(C1C2) bond in the pentagonal moiety and the two banana bonds τ_1(C2C3) and τ_2(C2C3). The picture in $B_{60}H_{60}$ is very similar, with a σ(B1B2) and two 3c-2e banana bonds τ_1(B2H_{in}B3) and τ_2(B2H_{out}B3). The presence of a F_{out} atoms in $B_{60}F_{30}H_{30}$ give additional LMOs due to the fluorine lone pairs: σ(2c-2e) = σ(B_1B_2), banana bond τ(3c-2e) = τ(B_2HB_3), σ(2c-2e) = σ(FB_2), σ(2c-2e) = σ(FB_3), F lone pair 1 and F lone pair 2; namely, instead of 3c-2e bonds, the BFB moiety consists of two σ(FB) bonds and two lone pairs on the fluorine atom. The same situation takes place for $B_{60}F_{60}$, with no 3c-2e bonds, and the 2c-2e LMO σ(B1B2) forming the B5 pentagons, with the remaining σ(BF) bonds and two LMOs for each fluorine atom corresponding to two lone pairs. Again, the structural stability of $B_{60}F_{60}$ can be attributed to the internal icosahedral distribution of Fin atoms as depicted in Figure 14.

The orbital energy diagram for all the systems around the frontier orbitals depicted in Figure 7 is quite intriguing. The HOMO-LUMO gaps in the boro-fullerenes are similar (9.3-10.6) and significantly larger by 2-3 eV as compared to C_{60}. However, none of these boro-fullerenes have ever been synthesized. Therefore apart from the kinetic aspect, we should consider the thermochemical aspect in the formation of these clusters. As shown above in Table 6, the estimated heats of formation for $B_{60}H_{60}$, $B_{60}F_{30}H_{30}$ and $B_{60}F_{60}$ are 5696 kJ·mol^{-1}, 3750 kJ·mol^{-1} and 12322 kJ·mol^{-1} respectively.

According to Figures 7-10, the electronic configurations (RHF/6-31G) of these clusters are C_{60} (… h_u^{10} t_{1u}^0 …); $B_{60}H_{60}$ (… h_u^{10} t_{1u}^0 …) which is isoelectronic with C_{60} ; $B_{60}F_{30}H_{30}$ (… h_u^{10} a_g^0 …) and finally in $B_{60}F_{60}$ (… g_g^8 a_g^0 …). Therefore the C_{60}, isoelectronic $B_{60}H_{60}$, and $B_{60}F_{30}H_{30}$ systems have a common h_u HOMO with multiplicity 5. This is interesting because transition-metal atoms with d^n electronic configurations do not split under an icosahedral field [54] and can be inserted inside the cage maintaining the 5-fold degeneracy of *d* orbitals. On the other hand the HOMO in $B_{60}F_{60}$ have g_g character with multiplicity 4. The LUMO in C_{60} and $B_{60}H_{60}$ are t_{1u} irreducible representations and therefore $C_{60}^{(3-)}$ and $B_{60}H_{60}^{(3-)}$ trianions should be stable as is the case of $C_{60}^{(3-)}$ with known salts of M_3C_{60}, with M an alkali metal atom [55-57]. Introduction of fluorine atoms leads to the interesting change in the LUMO to a singly degenerate a_g orbital and therefore to the potential existence of monoanions $B_{60}F_{30}H_{30}^{(-)}$ and $B_{60}F_{60}^{(-)}$.

The HOMO and LUMO shapes of the molecules – Figures 7-10 – differ mainly in the "pure" π patterns of C_{60}, with the cage being a "nodal surface". Concatenation of π and π* orbitals in ethylene, HOMO and LUMO respectively, in the C_{60} buckyball leads to the HOMO and LUMO orbitals in C_{60}. However, the HOMO and LUMO orbitals in B_2H_6 are

Preprints (www.preprints.org) | NOT PEER-REVIEWED | Posted: 13 April 2022 doi:10.20944/preprints202204.0115.v1

"in-plane" $\pi^{\perp}$ and π^* orbitals respectively. The same is valid for $H_2B(FH)BH_2$ and $H_2B(F_2)BH_2$ molecules, with HOMO and LUMO orbitals displayed in the SI file. Hence the HOMO in $B_{60}H_{60}$ and derivatives has no longer the icosahedral B_{60} skeleton as a nodal surface. However, the LUMO orbitals maintain the B_{60} skeleton as a "nodal surface" for all B_{60} systems. A very interesting point is the shape of the LUMO in $B_{60}F_{60}$, with large wave-function amplitudes pointing inwards the cage, which could stabilize a monoanion inside.

In the particular case of C_{60} *vs.* $B_{60}H_{60}$ as isostructural and isoelectronic systems, we applied the recently developed Hückeloid model for planar boranes [28] to $B_{60}H_{60}$ and compared to Hückel theory applied to C_{60}. The Hückel model is still applied for the analysis of novel conjugated systems, as recently shown [58]. In the SI file we collect the application of these two models with different basis sets, with excellent results for $B_{60}H_{60}$ regarding the fitting with *ab initio* orbital energy levels, as depicted in Figure 13. However, the Hückel model gives larger differences for the *ab initio* energy levels of C_{60}. The fact that the Hückeloid model can also be applied to a curved closed system such as the "spherical" $B_{60}H_{60}$ is an indication that larger "H-conjugated borane-type" systems in different dimensions could also be studied with this model.

Further analysis of the electronic structure through the density and its topological properties, give support to the previous analyses based on the electronic structure with orbitals and localized orbitals. The QTAIM description of the critical points of the electron density is gathered in Table 3. As expected, there are bond critical points (BCP) at the mid point of C1C2 and C2C3 bonds of C_{60}. Substitution of the "double" bond C1C2 by the B1(H2)B2 moiety gives a different picture: The bond path follows the B···H_{out}···B and B···H_{in}····B nuclei with a ring critical point (RCP) at about the center of the B($H_{in}H_{out}$)B rhombus. The B_5 pentagons show a BCP between any BB bond. Therefore, these analyses supports the construction of $B_{60}H_{60}$, a set of B5 pentagons joined by B(H2)B alternant moieties. The presence of fluorine atoms in $B_{60}F_{30}H_{30}$ does not change much the topological picture as compared to $B_{60}H_{60}$; in $B_{60}F_{60}$ more BCPs appear as interactions of the F_{in}···F_{in} neighboring atoms, as shown in Figure 14.

The most important information that can be extracted from the ELF is the localization of electrons. The striking point when looking at Figure 15, is the colour range differences observed between C_{60} and the boro-fullerenes. The electrons forming the C-C bonds are less localized between the two atoms as compared to those in the boron atoms, and thus the electron delocalization in C_{60} is lost in the boro-fullerenes. This last point and lower populations in the disynaptic basins coincides with a lower bond order for the B-B bond, as compared to the C-C bond. Another interesting point is the comparison of the three-center-bond ELF plots (Figure 16c, 16f, 16i). The B-H-B bonds are composed of more or less 2 electrons very localized between the boron and the hydrogen atoms. When replacing a hydrogen by a fluorine atom, the number of electrons in the V(B,B,H_{in}) basin increases, surely due to the low number, and poorly localized, electrons between the boron and fluorine atoms (1.48 electrons instead of 1.94). The substitution of the remaining hydrogens by a fluorine atoms increases the number of electrons between the F_{out} and the boron atoms (1.74 *vs* 1.48). The new link is similar to the one existing between F_{out} and the boron atoms in the $B_{60}F_{30}H_{30}$ compound. However the electrons in this system are not really localized between the fluorine and boron atoms. The fact that the electrons are more localized on the fluorine atoms than between the two atoms forming a bond, can also be confirmed on the hexagonal moiety ELF. Indeed, it can be established that, by increasing the number of fluorine atoms, the ELF value between the bridge-bonded boron atoms decreases from 0.7 to almost 0.0. The electrons are no longer localized in the ring plane, decreasing the bond order between the boron atoms and proving again the lack of delocalization in the boro-fullerene systems.

Previous studies of neutral *closo*-boranes B_nH_n , such as $B_{16}H_{16}$, $B_{19}H_{19}$ and $B_{22}H_{22}$ [34] calls for the comparison with $B_{60}H_{60}$, by means of the energy per BH unit and the binding energy - Eq.(6). Both methods give the following stability order $B_{16}H_{16}$ > $B_{22}B_{22}$ > $B_{19}H_{19}$ >

Preprints (www.preprints.org) | NOT PEER-REVIEWED | Posted: 13 April 2022 doi:10.20944/preprints202204.0115.v1

$B_{60}H_{60}$. A different order was obtained in Ref. [36] due to the lower accuracy of their over-simplified method. Therefore, although highly symmetrical, the icosahedral $B_{60}H_{60}$ cage is less stable than the smaller closo-boranes with n = 16, 19 and 22. Heats of formation were also computed for the boro-fullerenes as gathered in Table 6, which can be useful in the prediction for stability and synthesis of new (fluoro)borane-derived fullerenes.

4. Computational Methods

Geometry optimizations for C_{60} , $B_{60}H_{60}$, $B_{60}F_{60}$, $B_{60}(F_{30})_{out}(H_{30})_{in}$ and $B_{60}(F_{30})_{in}(H_{30})_{out}$ molecules as well as MEPs were computed at the B3LYP/cc-pVDZ level of theory [59-63] with the scientific software Gaussian16© [64]. All systems have icosahedral I_h symmetry and correspond to energy minima, checked with frequency computations, with the exception of $B_{60}(F_{30})_{in}(H_{30})_{out}$ – Figure 1d – that corresponds to a 7th-order saddle point. The Cartesian coordinates of all optimized geometries are included in the SI file. Foster–Boys localization and multicentric bond order indices were obtained from the Gaussian and Multiwfn computational packages, respectively [65,66], using a Restricted Hartree-Fock (RHF) wave function with the 6-31G basis set. Furthemore, multicentric bond order indices and the orbital energy levels around the frontier orbitals HOMO and LUMO were obtained from several basis sets for comparative purposes: STO-3G [67], 6-31G [68] and cc-pVDZ [63]. The Quantum Theory of Atoms in Molecules (QTAIM) [29,30] analysis of the electron density was carried out with the AIMAll scientific software [69]. For the ELF [34,35] computations we used the Multiwfn scientific software [70], with an electron density extracted from a B3LYP-cc-pVDZ wavefunction, a grid having a point every 0.03Å on the x, y, z axis, starting and finishing at the minima and maxima coordinates along the axis plus 2.5 Å, corresponding to more than 500 points along each axis. The Hückeloid model was applied for $B_{60}H_{60}$ with the t , t_b and ε_b parameters included in Ref. [28] for planar boranes. CCSD(T)-DLPNO computations [71] were carried out for the *closo*-boranes B_nH_n , with n = 16, 19, 22, 60, as gathered in Table 4 and Table 5.

5. Conclusions

The one-to-one correspondence between any conjugated hydrocarbon C_nH_m and its isoelectronic and isostructural borane analogue B_nH_{m+n} has been applied here to C_n conjugated systems – m = 0 – with the well-known Buckminsterfullerene C_{60} , leading to the boro-fullerene $B_{60}H_{60}$, previously studied. [38] Both systems have icosahedral symmetry Ih but reserve structural parameters: the double bonds in C_{60} are transformed into B(H2)B rhombus moieties with longer BB distances as compared to the single bond BB distances of the B5 pentagons in $B_{60}H_{60}$. Thus, $B_{60}H_{60}$ can be thought of as B5 pentagons joined by $B(H_2)B$ alternant moieties forming hexagons. We provide two new fluoro-borane-type fullerenes with all H_{in} and/or H_{out} substituted by fluorine atoms leading also to icosahedral I_h structures $B_{60}F_{30}H_{30}$ and $B_{60}F_{60}$. The structure with $B_{60}(F_{30})_{in}(H_{30})_{out}$ is a 7th – order saddle point, which collapses to a double-layered structure when removing the first imaginary vibrational frequency. All systems have 5-fold degenerate h_u orbitals as HOMO except $B_{60}F_{60}$ with a g_g orbital (degeneracy 4). thus, C_{60} with a triply degenerate LUMO leads to well-known stable trianions $C_{60}^{(3-)}$. However, for $B_{60}H_{60}$ and $B_{60}F_{30}H_{30}$, the LUMO levels and above are very close in energy and therefore one would expect stable polyanions. As for $B_{60}F_{60}$ the LUMO is of a_g nature and quite separated from other virtual orbitals in energy and therefore stable monoanions $B_{60}F_{60}^{(-)}$ are expected: moreover, the large wavefunction amplitude of the LUMO orbital pointing inwards is a clear indication of potential $X^{(-)}@B_{60}F_{60}$ stable systems, provided steric hindrance is avoided. The analysis through localized molecular orbitals and electron density with QTAIM and ELF theories gives a complementary view of the bonding in these systems, clearly showing that in the $B_{60}F_{30}H_{30}$ and $B_{60}F_{60}$ systems, no 3c-2e bonds take place in the B···F···B moieties. Finally, the heats of formations computed from experimental heats of formation of H(g), B(g), and F(g) and the computed enthalpies of reactants and products give some help in order to predict the stability and potential synthesis of the $B_{60}H_{60}$, $B_{60}F_{30}H_{30}$, and $B_{60}F_{60}$ clusters. We hope that

the results presented in this work can lead to new syntheses of boranes, different from the "classical" 3D open and closed (*closo*) polyhedral boranes.

Supplementary Materials: Table S1: Zero-point energy and thermal corrections for all systems; Table S2-S6: Cartesian coordinates (Å) for the optimized geometries of C_{60}, $B_{60}H_{60}$, $B_{60}F_{60}$, $B_{60}(F_{30})_{out}(H_{30})_{in}$ and $B_{60}(F_{30})_{in}(H_{30})_{out}$; Table S7: π-orbital energies (E_h) for the $B_{60}H_{60}$ molecule; Table S8: Exact Hückeloid model with shift to ½ ·|HOMO+LUMO| for energy levels in $B_{60}H_{60}$ for different basis sets; Figure S1: $B_{60}H_{60}$ π-orbital energy levels of the Hückeloid model and ab initio SCF computation (RHF) with different basis sets; Figure S2: frontier molecular orbitals for B_2H_6, B_2H_5F, $B_2H_4F_2$ and B_2F_6 molecules; Figures S3-S6: localized molecular orbitals for B_2H_6, B_2H_5F, $B_2H_4F_2$ and B_2F_6 molecules.

Author Contributions: Software, O.B.O. , M.F.; methodology, D.R.A, A.T., L.L., I.A., and G.E.M.; conceptualization, J.M.O.E., J.E., and I.A.; validation, J.M.O.E., I.A.; writing—original draft preparation, J.M.O.E.; writing—review and editing, I.A., J.E., M.F, D.R.A; project administration, I.A., D.R.A; funding acquisition, I.A., J.M.O.E.,D.R.A. All authors have read and agreed to the published version of the manuscript.

Funding: M. Ferrer, I. Alkorta, J. Elguero and J.M. Oliva-Enrich are grateful to Ministerio de Ciencia, Innovación y Universidades, for financial support with grant number PID2021-125207NB-C32. O.B. Oña, D.R. Alcoba, and G.E. Massaccesi acknowledge the financial support from the Universidad de Buenos Aires (Grant No. 20020190100214BA), the Consejo Nacional de Investigaciones Científicas y Técnicas (Grant Nos. PIP 11220200100467CO, PIP 11220130100377CO, and PIP 11220130100311CO), and the Agencia Nacional de Promoción Científica y Tecnológica, Argentina (Grant No. PICT-201-0381).

Data Availability Statement: In this section, please provide details regarding where data supporting reported results can be found, including links to publicly archived datasets analyzed or generated during the study. Please refer to suggested Data Availability Statements in section "MDPI Research Data Policies" at https://www.mdpi.com/ethics. If the study did not report any data, you might add "Not applicable" here.

Acknowledgments: In this section, you can acknowledge any support given which is not covered by the author contribution or funding sections. This may include administrative and technical support, or donations in kind (e.g., materials used for experiments).

Conflicts of Interest: The authors declare no conflict of interest.

References

1. Matsuda, I.; Wu. K (Eds). *2D boron: boraphene, borophene, boronene*; Springer Nature: Cham, Switzerland, 2021.
2. Cuxart, M. G.; Seufert, K.; Chesnyak, V.; Waqas, W. A.; Robert, A.; Bocquet, M.-L.; Duesberg, G. S.; Sachdev, H.; Auwärter, W. Borophenes made easy. *Sci. Adv.* **2021**, *7*, eabk1490, 1-7.
3. Jiao, Y.; Ma, F.; Bell, J.; Bilic, A.; Du, A. Two-dimensional boron hydride sheets: high stability, massless Dirac fermions, and excellent mechanical properties. *Angew. Chem.* **2016**, *128*, 10448–10451.
4. Shao, L.; Duan, X.; Li, Y.; Yuan, Q.; Gao, B.; Ye, H.; Ding, P. A theoretical study of several fully hydrogenated borophenes. *Phys. Chem. Chem. Phys.* **2019**, *21*, 7630-7634.
5. Poater, J.; Solà, M.; Viñas, C.; Teixidor, F. A simple link between hydrocarbon and borohydride chemistries. *Chem. Eur. J.* **2013**, *19*, 4169–4175.
6. Oliva-Enrich, J.M.; Alkorta, I.; Elguero, J.; Ferrer, M.; Burgos, J.I. On the 3D → 2D Isomerization of Hexaborane(12). Chemistry 492 2021, 3, 28-38.
7. Beckett, M.A. Boron Chemistry (IMEBORON XVI). *Chemistry International* **2017**, *39*, 44-45.
8. Kahl, S. B.; Kasar, R. A. Simple, High-yield synthesis of polyhedral carborane amino acids. *J. Am. Chem. Soc.* **1996**, *118*, 1223-1224.
9. Grimes, R.N. *Carboranes*, 3rd ed.; Academic Press: Cambridge, MA, USA, 2016.
10. Oliva-Enrich J. M.; Kondo, T.; Alkorta, I.; Elguero, J.; Klein, D. J. Title. Diborane concatenation leads to new planar boron chemistry. *Chem. Phys. Chem.* **2020**, *21*, 2460–2467.
11. Oliva-Enrich, J. M.; Alkorta, I.; Elguero, J. Hybrid Boron-Carbon Chemistry. *Molecules* **2020**, *25*, 5026.
12. Kroto, H. W.; Heath, J. R.; O'Brien, S. C.; Curl, R. F.; Smalley, R. E. C_{60}: Buckminsterfullerene. *Nature* **1985**, *318*, 162-163.
13. Quong, A. A.; Pederson, M. R.; Broughton, J. Q. Boron hydride analogues of the fullerenes. *Phys. Rev. B* **1994**, *50*, 4787-4794.
14. Ionov, S. P.; Kuznetsov, N. T. Heat of formation of boron hydride $B_{60}H_{60}$, an analog of fullerene C_{60}. The structural-thermochemical model. *Russian J. Coord. Chem.* **1995**, *21*, 845-849.

15. Derecskei-Kovacs, A.; Dunlap, B. I.; Lipscomb, W. N.; Lowrey, A.; Marynick, D. S.; Massa, L. Quantum chemical studies of boron fullerene analogs. *Inorg. Chem.* **1994**, *33*, 5617-5619.
16. Lipscomb, W. N.; Massa, L. Closo boron hydrides and carbon fullerenes. *Phosphorus, Sulfur, Silicon* **1994**, *87*, 125-128.
17. Boustani, I.; Rubio, A.; Alonso, J. A. Ab initio study of boron-hydrogen spheres. In *Contemporary boron chemistry*; Davidson, M.G., Wade, K., Marder, T.B., Hughes, A.K. (Eds.); RSC, Cambridge, Uk, 2000; pp. 493-496.
18. Gonzalez-Szwacki, N.; Sadrzadeh, A.; Yakobson, B. I. B_{80} Fullerene: An ab initio prediction of geometry, stability, and electronic structure. *Phys. Rev. Lett.* **2007**, *98*, 166804.
19. Murray, J. S.; Sen, K (Eds), Molecular electrostatic potentials: concepts and applications. M. Orozco, F. J. Luque, Generalization of the molecular electrostatic potential for the study of noncovalent interactions, *Theor. Comp. Chem.* **1996**, 3, 181-218.
20. Bausch, J.W.; Surya Prakash, G.K.; Olah, G.A.; Tse, D.S.; Lorents, D.C.; Bae, Y.K.; Malhotra, R. Considered novel aromatic systems. 11. Diamagnetic polyanions of the C_{60} and C_{70} fullerenes: preparation, ^{13}C and ^{7}Li NMR spectroscopic observation, and alkylation with methyl iodide to polymethylated fullerenes. *J. Am. Chem. Soc.* **1991**, *113*, 3205-3206.
21. Klaiman, S.; Gromov, E. V.; Cederbaum, L.S. All for one and one for all: accommodating an extra electron in C_{60}. *Phys. Chem. Chem. Phys.* **2014**, *16*, 13287-13293.
22. Mulliken, R. S. Electronic population analysis on LCAO–MO molecular wave functions. I. *J. Chem. Phys.* **1955**, 23, 1833-1840.
23. Mayer, I. Charge, bond order and valence in the ab initio SCF theory. *Chem. Phys. Lett.* **1983**, 97, 270-274.
24. Giambiagi, M.; de Giambiagi, M. S.; Mundium, K. C. Definition of a multicenter bond index. *Struct. Chem.* **1990**, 1, 423-427.
25. Ponec, R.; Roithová, J.; Sannigrahi, A. B.; Lain, L.; Torre, A.; Bochicchio, R. On the nature of multicenter bonding in simple atomic clusters. *J. Mol. Struct. (Theochem)* **2000**, 505, 283-288.
26. Torre, A.; Alcoba, D.R.; Lain,L.; Bochicchio, R.C. Determination of three-center bond indices from population analyses: a fuzzy atom treatment. *J. Phys. Chem. A* **2005**, 109, 6587-6591.
27. Foster, J. M.; Boyhys, S.F. Canonical configurational interaction procedure. *Rev. Mod. Phys.* **1960**, 32, 300-302.
28. Klein, D. J.; Ferrer, M.; Elguero, J.; Bytautas, L.; Oliva-Enrich, J. M. Hückeloid model for planar boranes. *Theor. Chem. Acc.* **2021**, *140*, 55:1-10.
29. Bader, R.F.W. *Atoms in Molecules: A Quantum Theory*; Clarendon Press: Oxford, UK, 1990.
30. Popelier, P.L.A. *Atoms in Molecules. An Introduction*; Prentice Hall: Harlow, UK, 2000.
31. Matta, C. F.; Castillo, N.; Boyd, R. J. Characterization of a closed-shell fluorine−fluorine bonding interaction in aromatic compounds on the basis of the electron density. *J. Phys. Chem. A* **2005**, *109*, 3669–3681.
32. Alkorta, I.; Elguero, J. Fluorine–fluorine interactions: NMR and AIM analysis. *Struct. Chem.* **2004**, *15*, 117–120.
33. Huber, K.P.; Herzberg, G., *Molecular spectra and molecular structure. IV. constants of diatomic molecules*; Van Nostrand Reinhold Co., 1979.
34. Becke, A.D.; Edgecombe, K.E. A simple measure of electron localization in atomic and molecular systems. *J. Chem. Phys.* **1990**, *92*, 5397–5403.
35. Silvi, B.; Savin, A. Classification of chemical bonds based on topological analysis of electron localization functions. *Nature* **1994**, *371*, 683–686.
36. Bicerano, J.; Marynick, D.S.; Lipscomb, W.N. Molecular Orbital Studies on Large Closo Boron Hydrides. *Inorg. Chem.* **1978**, *17*, 3443-3453.
37. Bhattacharyya, P.; Boustani, I.; Shukla, A. Why Does a $B_{12}H_{12}$ Icosahedron Need Two Electrons to be Stable: A First-Principles Electron-Correlated Investigation of $B_{12}H_n$ (n = 6, 12) Clusters. *J. Phys. Chem. A* **2021**, *125*, 10734-10741.
38. Ionov, S.P.; Kuznetsov, N.T. Heat of Formation of Boron Hydride $B_{60}H_{60}$, an Analog of Fullerene C_{60}. The Structural-Thermochemical Model. *Russian J. Coord. Chem.* **1995**, *21*, 883-887.
39. Chase, M.W., Jr., NIST-JANAF Themochemical Tables, Fourth Edition, *J. Phys. Chem. Ref. Data*, Monograph 9, 1998, 1-1951.
40. Iijima, S. Helical microtubules of graphitic carbon. *Nature* **1991**, 354, 56–58.
41. Stock, A. The hydrides of boron and silicon. Cornell University Press, New York, USA, 1933.
42. Lewis, G.N. The Atom and the Molecule. *J. Am. Chem. Soc.* **1916**, *38*, 762–785.
43. Mingos, D.M.P, Ed. 50th anniversary of electron counting paradigms for polyhedral molecules. Springer, Cham, Switzerland, 2021.
44. Muetterties, E.L., (Ed.) *Boron Hydride Chemistry*; Academic Press, NY, 1975.
45. Lipscomb, W.N. *Boron Hydrides*; Dover, NY, 2012.
46. Nishino, H.; Fujita, T.; Cuong, N.T.; Tominaka, S.; Miyauchi, M.; Iimura, S.; Hirata, A.; Umezawa, N.; Okada, S.; Nishibori, E.; Fujino, A.; Fujimori, T.; Ito, S.; Nakamura, J.; Hosono, H.; Kondo, T. *J. Am. Chem. Soc.* **2017**, *139*, 13761–13769.
47. Alexandrova, A.N.; Birch, K.A.; Boldyrev, A.I. Flattening the $B_6H_6^{2-}$ Octahedron. Ab Initio Prediction of a New Family of Planar All-Boron Aromatic Molecules. *J. Am. Chem. Soc.* **2003**, 125, 36, 10786–10787.
48. Yanonni, C.S.; Bernier, P.P.; Bethune, D.S.; Meijer, G.; Salem, J.K. NMR determination of the bond lengths in C_{60}. *J. Am. Chem. Soc.* **1991**, *113*, 3190-3192.
49. Hedberg, K.; Schomaker, V. Reinvestigation of the structures of diborane and ethane by electron diffraction. *J. Am. Chem. Soc.* **1951**, *73*, 1482-1487.
50. Alkorta, I.; Soteras, I.; Elguero, J.; Del Bene, J.E. The boron–boron single bond in diborane(4) as a non-classical electron donor for hydrogen bonding. *Phys. Chem. Chem. Phys.* **2011**, 13, 14026–14032.
51. Treboux, G.; Barthelat, J.C. X-X direct bonds versus bridged structures in group 13 X_2H_2 potential energy surfaces. *J. Am. Chem. Soc.* **1993**, *115*, 4870–4878.

52. Greenwood, N.N.; Earnshaw, A. *Chemistry of the Elements* (2nd ed.); Butterworth-Heinemann, 1997.
53. Montero-Campillo, M.M.; Alkorta, I.; Mó, O.; Elguero, J.; Yáñez, M. Clustering of electron deficient B- and Be-containing analogues: in the fight for tetracoordination, Beryllium takes the lead, *Eur. J. Inorg. Chem.* **2021**, 4393–4401.
54. Plakhutin, B.N. D. Sc. thesis, Moscow State University, 1995.
55. Liu, X.; Wan, W. C.; Owens, S. M.; Broderick, W. E. Superconducting alkali metal fullerides: development of a versatile solution-phase route from soluble M_3C_{60} precursors. *J. Am. Chem. Soc.* **1994**, *116*, 5489-5490.
56. Kobayashi, H.; Tomita, H.; Moriyama, H.; Kobayashi, A.; Watanabe, T. New metallic C_{60} compound: $Na_xC_{60}(THF)_y$. *J. Am. Chem. Soc.* **1994**, *116*, 3153-3154.
57. Chen, J.; Huang, Z.-E. ; Cai, R.-F. ; Shao, Q.-F.; Chen, S.-M.; Ye, H.-J. A new method for the preparation of fullerene anion salts: synthesis and characterization of $KC_{60}(THF)$. *J. Chem. Soc., Chem. Commun.* **1994**, 2177-2178.
58. Apriliyanto, Y. B.; Battaglia, S.; Evangelisti, S.; Faginas-Lago, N.; Leininger, T.; Lombardi, A. Toward a generalized Hückel rule: The electronic structure of carbon nanocones. *J. Phys. Chem. A* **2021**, *125*, 9819–9825.
59. Becke, A.D. Density-functional thermochemistry. III. The role of exact exchange. *J. Chem. Phys.* **1993**, *98*, 5648-5652.
60. Lee, C.; Yang, W.; Parr, R.G. Development of the Colle-Salvetti correlation-energy formula into a functional of the electron density. *Phys. Rev. B* **1988**, *37*, 785-789.
61. Vosko, S.H.; Wilk, K.; Nusair, M. Accurate spin-dependent electron liquid correlation energies for local spin density calculations: a critical analysis. *Can. J. Phys.* **1980**, *58*, 1200-1211.
62. Stephens, P.J.; Devlin, F.J.; Chabalowski, C.F.; Frisch, M.J. Ab initio calculation of vibrational absorption and circular dichroism spectra using density functional force fields. *J. Phys. Chem.* **1994**, *98*, 11623-11627.
63. Dunning Jr., T.H. Gaussian basis sets for use in correlated molecular calculations. I. The atoms boron through neon and hydrogen. *J. Chem. Phys.* **1989**, *90*, 1007-1023.
64. Gaussian 16, Revision C.01, Frisch, M. J.; Trucks, G. W.; Schlegel, H. B.; Scuseria, G. E.; Robb, M. A.; Cheeseman, J. R.; Scalmani, G.; Barone, V.; Petersson, G. A.; Nakatsuji, H.; Li, X.; Caricato, M.; Marenich, A. V.; Bloino, J.; Janesko, B. G.; Gomperts, R.; Mennucci, B.; Hratchian, H. P.; Ortiz, J. V.; Izmaylov, A. F.; Sonnenberg, J. L.; Williams-Young, D.; Ding, F.; Lipparini, F.; Egidi, F.; Goings, J.; Peng, B.; Petrone, A.; Henderson, T.; Ranasinghe, D.; Zakrzewski, V. G.; Gao, J.; Rega, N.; Zheng, G.; Liang, W.; Hada, M.; Ehara, M.; Toyota, K.; Fukuda, R.; Hasegawa, J.; Ishida, M.; Nakajima, T.; Honda, Y.; Kitao, O.; Nakai, H.; Vreven, T.; Throssell, K.; Montgomery, J. A., Jr.; Peralta, J. E.; Ogliaro, F.; Bearpark, M. J.; Heyd, J. J.; Brothers, E. N.; Kudin, K. N.; Staroverov, V. N.; Keith, T. A.; Kobayashi, R.; Normand, J.; Raghavachari, K.; Rendell, A. P.; Burant, J. C.; Iyengar, S. S.; Tomasi, J.; Cossi, M.; Millam, J. M.; Klene, M.; Adamo, C.; Cammi, R.; Ochterski, J. W.; Martin, R. L.; Morokuma, K.; Farkas, O.; Foresman, J. B.; Fox, D. J. Gaussian, Inc., Wallingford CT, 2016.
65. Schmidt, M. W.; Baldridge, K. K.; Boatz, J. A.; Elbert, S. T.; Gordon, M. S.; Jensen, J. H., Koseki, S.; Matsunaga, N.; Nguyen, K. A.; Su, S.; Windus, T. L.; Dupuis, M.; Montgomery, J. A. General atomic and molecular electronic structure system. *J. Comput. Chem.* **1993**, *14*, 1347-1363.
66. Lu, T.; Chen, F. J. Multiwfn: A multifunctional wavefunction analyzer. *J. Comput. Chem.* **2012**, *33*, 580-592.
67. Collins, J.B.; Schleyer, P.v.R.; Binkley, J.S.; Pople, J.A. Self-consistent molecular orbital methods. XVII. Geometries and binding energies of second-row molecules. A comparison of three basis sets. *J. Chem. Phys.* **1976**, *64*, 5142.
68. V. A. Rassolov, V.A.; M. A. Ratner, M.A.; J. A. Pople, J.A.; P. C. Redfern, P.C.; and L. A. Curtiss, L.A. 6-31G* basis set for third-row atoms. *J. Comp. Chem.* **2001**, *22*, 976-84.
69. Keith, T.A. AIMAll; Version 19.10.12; TK Gristmill Software: Overland Park, KS, USA, 2017.
70. Lu, T.; Chen, F. Multiwfn: A multifunctional wavefunction analyzer. *J. Comput. Chem.* **2012**, *33*, 580-592.
71. Guo, Y.; Riplinger, C.; Becker, U.; Liakos, D. G.; Minenkov, Y.; Cavallo, L.; Neese, F. Communication: An improved linear scaling perturbative triples correction for the domain based local pair-natural orbital based singles and doubles coupled cluster method [DLPNO-CCSD(T)]. *J. Chem. Phys.* **2018**, *148*, 011101.